Investigating the effects of living with HIV on neural circuits involved in reward processing in adolescents

By Anika Mac Arthur

MCRANI001

In fulfilment of the requirements for the degree of Masters of Science in Biomedical Engineering

Faculty of Health Sciences

UNIVERSITY OF CAPE TOWN

June 2024

Supervisor: Prof. Ernesta Meintjes

Co-Supervisor: Dr Frances Robertson

Declaration

I, ANIKA MAC ARTHUR, hereby declare that the work on which this thesis is based is my own original work (except where acknowledgements indicate otherwise) and that neither the whole, nor any part of it, has been, or is to be submitted for any other degree in this or any other University.

I empower the University to reproduce, for the purpose of research, either the whole of part of the content of this thesis in any manner.

Signed by candidate

Signature

11 June 2024

Date

Acknowledgements

Support for this study was provided by NIH grants R01HD099846, R01DC015984, R01HD071664, R21MH108346 and R21MH096559; South African National Research Foundation (NRF) grants 48337, 99069 and 78737; UCT VC Interim Funding; US National Institute of Allergy and Infectious Diseases (NIAID) through the CIPRA network, Grant number U19AI53217; and the South African Medical Research Council (MRC). We wish to acknowledge the contribution of the following to this study: Staff of the Family Centre for Research with Ubuntu (FAMCRU), Tygerberg Children's Hospital, Cape Town, South Africa; Staff of the Cape Universities Body Imaging Centre (CUBIC), Cape Town, South Africa; the children who participated in this study and their caregivers.

Furthermore, I, Anika, wish to thank my supervisors for their support throughout the completion of this degree. I would also like to thank my family for motivating me and keeping me accountable. Lastly, I would like to thank our Heavenly Father for the grace He has given me to, firstly, be in this privileged position to complete this degree, as well as providing me with the support system He knew I needed.

Soli Deo Gloria

Abstract

The CHER (Children with HIV Early Antiretroviral) trial found that early ART (≤12-weeks) reduced mortality and morbidity in children with perinatal HIV (CPHIV). Despite early ART, CPHIV from the CHER trial demonstrate neuroimaging alterations, but little is known about the effects of PHIV and long-term ART on the adolescent brain. Adolescence is a time of increased vulnerability to risk-taking behaviour. Here, neural circuits involved in reward processing during adolescence are investigated using functional MRI (fMRI).

FMRI scans acquired during a Reward Magnitude Task were available for 106 socio-economically matched adolescents (66 children perinatally infected with HIV (CPHIV), 40 controls living without HIV; age 15±0.4 years). Data were preprocessed using fMRIPrep. Differences in brain activation for anticipation, monetary wins vs losses, and reward/loss outcome magnitudes were compared between CPHIV and controls using FSL FEAT. Z-statistic images were thresholded at Z>3.1 and a cluster significance threshold of p=0.05.

Across all subjects, there were robust responses to reward processing (win>loss) in the striatum (38,610mm^3; peak MNI -10.1; 9.1; 0.7) and in the (ventromedial) prefrontal cortex (11,280mm^3; peak MNI -5.3; 25.9; 41.5). There were no regions where activation increases, for any of our contrasts, were greater in CPHIV than controls, but CPHIV showed smaller activation increases than controls during anticipation and reward processing. We specifically saw smaller activation increases during processing of larger wins in 2 distinct small left superior frontal clusters as well as in the left paracingulate gyrus.

Similar to findings from the Human Connectome Project in Development, the task reliably activated striatal and medial frontal regions involved in decision-making and reward seeking/processing. While we found no differences between CPHIV and controls within this reward processing network, CPHIV showed smaller activation differences in our contrasts in the left superior frontal cortex – a region involved in the working memory component of executive function. Notably, impaired working memory processing and storage, especially in the visual domain, has been reported previously in children living with HIV. The current finding suggests that HIV-related brain response abnormalities in working memory regions may impact reward processing.

Table of Contents

Table of Figures

Table of Tables

List of Abbreviations

HIV	Human Immunodeficiency Virus
ART	Antiretroviral Therapy
BBB	Blood-Brain-Barrier
BOLD	Blood Oxygenation Level Dependent
PHIV	Perinatal Human Immunodeficiency Virus
ARV	Antiretroviral
HCP-D	Human Connectome Project in Development
MRI	Magnetic Resonance Imaging
fMRI	Functional Magnetic Resonance Imaging
CHER	Children with HIV Early Antiretroviral
ART-def	deferred Antiretroviral Therapy
ART-40W	Antiretroviral Therapy for 40 weeks
ART-96W	Antiretroviral Therapy for 96 weeks
WMSA	white matter signal abnormalities
WM	White Matter
CNS	central nervous system
CPHIV	Children Perinatally infected with HIV
CUBIC	Cape Universities Body Imaging Centre
UCT	University of Cape Town
TR	Repetition Time
TE	Echo Time
TI	Inversion Time
FOV	Field of View
EPI	Echo Planar Images
BW	Bandwidth
GLM	Generalised Linear Model
ROI	Region of Interest

1. Introduction

The Human Immunodeficiency Virus (HIV) is known to be one of humanity's most devastating epidemics. HIV attacks healthy cells in the human body that are responsible for fighting infections. When these cells are infected with HIV, they are no longer able to protect the body against infections, making such an individual more vulnerable to other infections and diseases. HIV is most commonly spread from an infected individual through certain bodily fluids, through the sharing of needles, or vertically from mother to child during pregnancy, delivery or breastfeeding (HIV.gov, 2020, Le Doare et al., 2012). A person infected via the latter mode is referred to as having perinatal HIV infection (PHIV).

In 2020, there were 37.7 million people globally living with HIV (UNAIDS, 2021b), of which 20.6 million live in Eastern and Southern Africa (UNAIDS, 2021c). In South Africa alone, there were about 7.8 million people living with HIV of whom 310 000 were children between ages 0 and 14 years (UNAIDS, 2021a).

Fortunately, antiretroviral therapy (ART) coverage among people living with HIV increased by about 50% over the last decade (UNAIDS, 2021d).

Although antiretrovirals (ARVs) circulating in the peripheral blood adequately suppress the HIV virus and the replication thereof in the periphery, few ARVs cross the blood-brain-barrier (BBB). This causes the brain to become a safe haven for HIV from where it infects the brain (Osborne et al., 2020). It is thus important to initiate ART as soon as possible to prevent, or limit, HIV from crossing the BBB and resultant neuroinflammation and/or brain damage which may impact neurodevelopment (Lorin et al., 2020).

The fact that most children with PHIV (CPHIV) start ART soon after diagnosis, has given rise to a new generation of children growing up on ART. Despite being virally suppressed, these children and adolescents continue to demonstrate deficits or delays on neurocognitive assessments (Boivin et al., 2018, Laughton et al., 2013) and alterations on neuroimaging (Herting et al., 2015, Lewis-de Los Angeles et al., 2020).

It is also common for adolescents with PHIV to perform more poorly on tests of general intellectual functioning and to have repeated grades at school (Hoare et al., 2018). It is not clear

whether these are a consequence of early damage, before initiating ART, or ongoing HIV-related damage. Although early combination ART improves cognitive outcomes (Laughton et al., 2018), more data are needed pertaining to the long-term effects of living with HIV on the developing brain (van Wyhe et al., 2021), and the consequences for adolescence (Laughton et al., 2013).

Adolescence is a time of increased vulnerability to risk-taking behaviour, impulsivity, and recklessness. Some of these risky behaviours include, but are not limited to, experimentation with drugs and alcohol, dangerous driving and unsafe sexual practices (Telzer et al., 2013). This period poses particular challenges for adolescents living with PHIV who are additionally navigating the implications of their HIV status and greater responsibility for their own disease management. Moreover, vulnerability to risk-taking behaviour may be exacerbated by HIV-related neurodevelopmental deficits or delays (Laughton et al., 2013).

In 2018, Somerville et al. conducted The Lifespan Human Connectome Project in Development (HCP-D) – a cross-sectional study consisting of more than 1300 healthy individuals aged 5-21 years. The aim of this study was to obtain a better understanding of the healthy developing brain by means of imaging, especially during puberty. Functional MRI (fMRI) acquisition while performing the Reward Magnitude ("guessing") task, was used to measure neural responses to receipt of rewards and punishments (loss), neural activity that tracks reward and punishment magnitudes, and neural activity in anticipation of low and high magnitude outcomes. FMRI measures changes in the Blood Oxygenation Level Dependent (BOLD) signal. These changes occur due to the fact that the local magnetic field changes when blood oxygenation levels change in response to neural activity (Buxton, 2002). Using fMRI, Somerville et al. (2018) demonstrated robust responses for monetary wins relative to monetary losses in the dorsal- and ventral striatum, and the ventromedial prefrontal cortex - both of which are related to reward-seeking behaviour and decision-making (Baars, 2018, Goddings et al., 2014).

In the present study, we aimed to examine, by means of the Reward Magnitude task and fMRI, whether living with PHIV alters the neural pathways involved during adolescence in processing of reward and punishment as this may impact reward-seeking decisions. In view of evidence of ongoing neuroinflammation in PHIV from ages 5-11 years in the basal ganglia (van Biljon et al.,

2021), we hypothesize that adolescents living with PHIV would demonstrate reduced activation of the striatum during reward processing.

2. MRI Theory

Magnetic Resonance Imaging (MRI) has completely transformed our ability to study the structure and function of the human brain. The underlying principles of MRI are quite straightforward. In most cases, the MRI signal is based on the magnetic properties of hydrogen nuclei, which are abundant in the human body, and specifically in water.

When an individual undergoes an MRI scan, they are placed in a strong static magnetic field. This causes the dipole moments associated with their body's positively charged spinning hydrogen nuclei, which possess net angular momentum, to precess around the axis of the external static magnetic field at a characteristic frequency known as the Larmor precession frequency. The Larmor precession frequency is directly proportional to the strength of the magnetic field. These millions of precessing dipole moments result in a net magnetization parallel to the static field. When a small alternating magnetic field, called a radiofrequency (RF) pulse, is applied briefly at the Larmor precession frequency and perpendicular to the strong magnetic field, the dipole moments associated with the hydrogen nuclei in the body respond by precessing around the new net magnetic field. This causes the net magnetization resulting from the millions of precessing dipole moments to rotate away from being aligned parallel to the strong magnetic field – a process called excitation. After the RF pulse, as the dipole moments again start precessing around the strong magnetic field and return to their original orientations – a process called relaxation – the transverse components of their magnetization vectors induce a signal in a receiving coil. This signal is the MRI signal. The time constants T1 and T2 characterize the relaxation rate of the longitudinal and transverse components of the magnetization, respectively. T1, the spin-lattice relaxation rate, is defined as the time when 63% of the maximum longitudinal magnetization has been recovered. T2, the spin-spin relaxation rate, is the time when 63% of the transverse magnetization has dephased. By varying the static magnetic field at different positions, which spatially varies the precessional frequencies of the dipole moments, the spatial origin of the signal can be determined, ultimately allowing the creation of a three-dimensional image.

For imaging the structure of the brain, common MRI techniques include T1-weighted (T1W) and T2-weighted (T2W) images, diffusion tensor imaging (DTI), and magnetization transfer imaging (MT). These techniques help quantify the volume of grey and white matter, assess the cortical

thickness and folding, white matter microstructure, and other morphological properties of the cerebral cortex. In addition to these, there are less common but informative techniques such as magnetic resonance spectroscopy which provide insights into brain metabolism.

With MRI it is also possible to study brain function. A key parameter measured in functional MRI (fMRI) is the Blood Oxygenation-Level Dependent (BOLD) signal. This signal reflects the proportion of oxygenated and de-oxygenated blood in a specific brain region at a given moment. Functional Magnetic Resonance Imaging (fMRI) therefore indirectly measures neural activity by observing associated hemodynamic changes. The ability of fMRI to map overall brain activation related to specific tasks, combined with its non-invasive nature, makes it an invaluable tool for investigating cognitive and emotional processes.

3. Background

It is known that adolescents infected with HIV are more likely to have repeated grades at school (Hoare et al., 2018). This might be due to a combination of several aspects, such as the early neural damage caused by perinatally acquired HIV, the continuous presence of and infection by HIV in the adolescent body and brain, and the socioeconomic circumstances these adolescents find themselves in (Laughton et al., 2013).

In adolescents who started ART during childhood, HIV-related cognitive deficits persist (Puthanakit et al., 2010, Ezeamama et al., 2016). They also demonstrate compromised white matter integrity (Hoare et al., 2018) and reduced grey matter volumes and gyrification (Lewis-de Los Angeles et al., 2020) on neuroimaging.

The Children with HIV Early Antiretroviral (CHER) trial was a randomized controlled trial that enrolled asymptomatic infants younger than 12 weeks and perinatally infected with HIV. Interim data showed that the early initiation of ART (< age 12 weeks) reduced mortality rates. A reduction in HIV disease progression was also observed and it was concluded that the early initiation of ART was both safe and advantageous. As a result of these findings, in 2013, immediate initiation of ART became standard of care (Cotton et al., 2013, Lowenthal et al., 2014).

Another study investigating ART in infants and young children was the P1060 study of the International Maternal Pediatric Adolescent AIDS Clinical Trials Network (IMPAACT). The IMPAACT study was comprised of two parallel randomized trials involving ART eligible infants and young children between the ages of 2 months to 3 years. Between November 2006 and March 2010, 452 participants across 9 sites in Africa and 1 site in India were randomized to receive one of two ART regimens. CD4 percentages (CD4%) in both cohorts were extensively followed and monitored (Barlow-Mosha et al., 2016).

The major difference between the CHER and IMPAACT trials was that CPHIV from the IMPAACT trial started ART when clinically indicated, while CPHIV from the CHER trial started ART according to the treatment arm they had been randomized to, irrespective of their viral load or CD4% (as long as inclusion criteria were met).

A study by Ackermann et al. (2014) on the Cape Town-based infants from the CHER trial at mean age 31.9 months (roughly 2.5 years of age) demonstrated white matter signal abnormalities (WMSA) in 50% of infants. These findings suggest that white matter (WM) alterations occur very early in infancy and that initiating ART at around 8 weeks may still be too late to prevent the HIV from infecting the central nervous system (CNS) and crossing the BBB (Ackermann et al., 2014). Regional white matter alterations compared to uninfected controls continued to be evident in these children at ages 5 (Ackermann et al., 2016) and 7 years (Jankiewicz et al., 2017). Moreover, Mbugua et al. (2016) demonstrated higher levels of creatine, choline and glutamate in the basal ganglia at age 5 years in children from the CHER trial who received ART before 12 weeks of age compared to those who received ART after 12 weeks of age, and lower ratios of CD4 to CD8 around age 6 weeks were related to lower levels of N-acetylaspartate (NAA) and choline at age 5 years across all CPHIV, irrespective of timing of treatment initiation. While these findings suggest that earlier ART initiation purveys neurometabolic advantages for newborns, effects of immune compromise before 6-8 weeks seem to persist into early childhood (Mbugua et al., 2016). A follow-up study by Robertson et al. (2018) at ages 7 to 9 indicated that basal ganglia neurons may be particularly affected by PHIV and that neural damage may be ongoing despite early ART (Robertson et al., 2018). Structurally, Randall et al. found that 5-year-old CPHIV who initiated ART after 12 weeks showed larger volumetric differences compared to uninfected controls and in more subcortical regions than CPHIV who received ART prior to 12 weeks. Their results suggest that HIV-related damage is ongoing despite early ART initiation, but that earlier treatment is neuroprotective (Randall et al., 2017). In a follow-up study with the CHER cohort at age 7, Nwosu et al. similarly concluded that some neural structures are sensitive to timing of ART initiation (Nwosu et al., 2018).

At the 7- and 9-year follow-up of children from the CHER trial, they performed worse than their uninfected peers on working memory and executive function at both ages. Although the neurocognitive developmental trajectories observed from ages 7 to 9 were largely similar across groups, the author concluded that children with PHIV, regardless of their treatment arm, remain at risk for cognitive deficits during early adolescence (van Wyhe et al., 2021). This was also the main finding in the Peadiatric Randomized Early versus Deferred Initiation in Cambodia and Thailand (PREDICT) study conducted in 2012 (Puthanakit et al., 2012).

To date, due to the paucity of data specific to adolescents (Laughton et al., 2013), it is not known whether differences and deficits seen in childhood persist or resolve in these early-treated children as they enter adolescence, or whether there will be ongoing damage. Following these children into adolescence will elucidate whether changes observed in childhood represent developmental delay or HIV associated damage, which could be early or ongoing.

Adolescence is a developmental period characterized by risk-taking and reward-seeking behaviours as well as greater interest in social relationships, such as the experimentation with drugs and alcohol and sexual relationships among peers (Galvan, 2010, Galvan et al., 2012, Telzer et al., 2013).

Dealing with these challenges may be exacerbated by HIV-related brain damage. Adolescents living with HIV have to deal with additional challenges that potentially place them at greater risk. These include dealing with their chronic illness, confronting psychosocial issues and maintaining ART adherence. They are often faced with illness and death of their parents and siblings, stigma and discrimination, the confrontation of their own mortality and the pressing uncertainty of their future. They may also become responsible for younger siblings and other ill family members (Lowenthal et al., 2014). Even though family obligations have been associated with reduced likelihood of drug use and irresponsible behaviour (Telzer et al., 2013), family pride, unity and social support are often lacking, resulting in rebellion against family obligations. Loss of effective guidance and supervision, psychological distress, poor mental health, and loss of educational opportunities, may lead to high rates of risk-taking behaviours (Cluver et al., 2012). It is therefore important to investigate the impact of living with HIV on neural circuits associated with reward seeking and decision-making.

The human brain is highly complex with intricate and delicate connections. Functions are vast and interconnected. There are many studies that help us understand the complex human brain, specifically with regards to reward processing and the neural networks involved therein (Kruithof et al., 2023, Van Leijenhorst et al., 2010a, Van Leijenhorst et al., 2010b, Telzer et al., 2016, Sinai, 2018, Lesage et al., 2016, Somerville et al., 2018). The primary brain regions associated with reward processing form part of the dopamine pathways, also known as the reward pathways.

Figure 1 shows the four dopamine pathways in the brain. Both the striatum and the prefrontal cortex play key roles in the brain reward pathways. The ventral striatum consisting of the nucleus accumbens forms part of the mesolimbic pathway and the prefrontal cortex forms part of the mesocortical pathway. Together these regions form the mesocorticolimbic (MCL) system. The dorsal striatum, composed of the caudate nucleus and putamen, forms part of the nigrostriatal pathway (Lesage, 2016). These three dopaminergic pathways are directly involved in reward processing. The final pathway, known as the tuberoinfundibular pathway, regulates prolactin secretion by the pituitary gland and is not involved during reward processing.

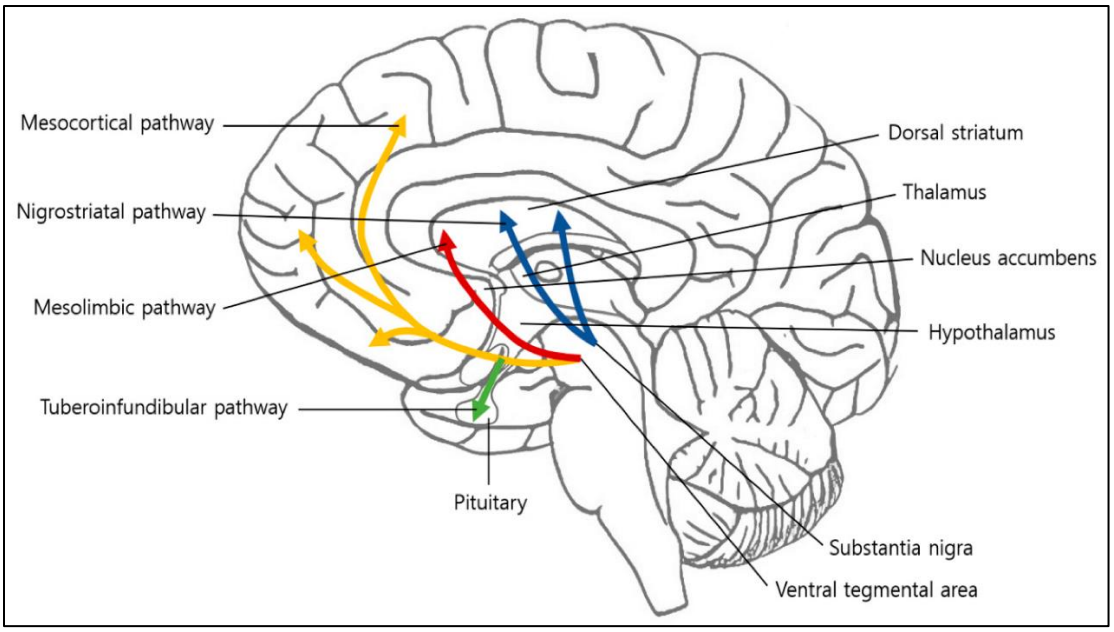

Figure 1: Four dopamine pathways in the brain (Yang et al., 2020)

The mesolimbic pathway (red in Figure 1) primarily projects from the ventral tegmental area (VTA) (found in the midbrain and primarily involved in limbic processes) to the ventral striatum, amygdala and hippocampus and is considered the reward hub where reward is primarily processed. The mesocortical pathway (yellow) also stems from the VTA, but then projects through the ventral striatum towards the prefrontal cortex where reward value is anticipated and processed. Finally, the nigrostriatal pathway (blue) stems from the substantia nigra pars compacta (which is also found in the midbrain, but more engaged in motor and cognitive

processes) and then projects to the dorsal striatum. This pathway is considered the “habit hub” of cognitive associations. After repetitive responses to a reward stimulus, which originally primarily occur in the ventral striatum (and project through the mesocorticolimbic system), conditioning takes place. When the response becomes habitual, neurons in the dorsal striatum are activated.

It is important to note that although there are distinct differences between the different dopamine pathways, they are all related to each other in some way or another. For instance, since projections to or through the striatum are common to various pathways, overlap is inevitable. Therefore, signals present in the limbic loop/pathway can impact signals in the cognitive loop/pathway, and vice versa (Lesage, 2016).

Du Plessis et al. (2015) conducted a study where they investigated the effects of HIV infection on reward processing by examining the function of the ventral–striatal reward system during a monetary incentive delay task using a sample of 34 adult participants, of which 18 were persons living with HIV. They found that participants living with HIV had less activation in the ventral striatum during cue processing (anticipation), but the same amount of activation than controls during processing of outcomes (reward). They also found no difference between groups during reward processing in the oribito-frontal cortex, which was one of the two regions of interest in their study (Du Plessis et al., 2015). It is worth noting that, in their cohort, the participants living with HIV were all adults newly diagnosed with HIV and not perinatally infected with HIV. These findings therefore do not provide information regarding the long-term effects of living with HIV in the early ART era. In a systematic review and meta-analysis by the same authors of fMRI studies examining effects of HIV infection on the fronto-striatal system, it was found that HIV particularly influences the executive control networks across a variety of tasks (Du Plessis et al., 2014). It is worth noting that only adult studies were considered.

To the author’s knowledge, the effects of living with HIV infection on neural circuits involved in reward processing, which may have an impact on risk-taking behaviour and decision-making, have not been studied in adolescents with PHIV.

4. Methodology

4.1 Participants

Participants were 129 socioeconomically matched adolescents with and without HIV (83 PHIV, 76 female) who received MR neuroimaging at the Cape Universities Body Imaging Centre (CUBIC). Data from 5 participants (3 PHIV) were discarded due to being incomplete and from a further 18 participants (14 PHIV) due to motion in the MRI scanner exceeding 3 mm displacement. We therefore present data for 106 participants (66 children perinatally infected with HIV (CPHIV), 40 controls living without HIV; mean age ± standard deviation 15.1±0.4 years; 45 males, 61 females). The smaller size of the control group is a consequence of higher attrition rates among controls for whom there is no direct benefit due to study participation; CPHIV receive clinical care and support through study participation. Of the 66 CPHIV, 57 were from the CHER (Children with HIV Early antiRetroviral) trial, and 9 from IMPAACT (International Maternal Pediatric Adolescent AIDS Clinical Trials Network). The major difference between children from these two cohorts is that those from CHER started ART according to the treatment arm they had been randomized to (i.e. either around age 6-12 weeks or when clinically indicated) compared to those from IMPAACT who started ART when clinically indicated (age 22-88 weeks [5-22 months]).

4.2 Procedure

Adolescents and their parents/guardians were transported by the research team to the Cape Universities Body Imaging Centre (CUBIC) located at Groote Schuur Hospital for neuroimaging assessments. The study was conducted according to protocols that had been approved by the Human Research Ethics Committees of the Faculties of Health Sciences of both the Universities of Cape Town and Stellenbosch. All parents/guardians and the adolescents provided written informed consent. Prior to scanning, the participants were introduced to the scanning environment using a mock scanner. This was important in reducing anxiety and facilitating completion of the MRI scans. The functional MRI tasks were also explained to participants and they were able to practice short versions of the tasks while in the mock scanner. In some cases, the parent/guardian was present in the MRI room to support the adolescent during the scanning procedure. An array of sequences was acquired, including structural and functional acquisitions.

4.3 Neuroimaging Assessment

4.3.1 Magnetic Resonance imaging protocol

All scans were acquired using the 3T MAGNETOM Skyra MRI scanner (Siemens, Erlangen, Germany) at CUBIC. High-resolution anatomical images were acquired using a three-dimensional inversion recovery gradient echo sequence. Imaging parameters were: 176 slices, TR = 2530 ms, TEs = 1.69/3.54/5.39/7.24 ms, TI = 1100 ms, slice thickness 1 mm, FOV 224 x 224 mm^2, 1 x 1 x 1 mm^3 resolution.

For functional MRI (fMRI), 270 T2*-weighted echo-planar (EPI) images were acquired with the multi-band EPI sequence from the University of Minnesota Center for Magnetic Resonance Research (Feinberg et al., 2010, Moeller et al., 2010, Xu et al., 2013) while participants performed the Reward Magnitude ("guessing") task (Somerville et al., 2018). Imaging parameters were: FOV 216 x 216 mm^2, 60 interleaved slices, 2.4 x 2.4 x 2.4 mm^3 isotropic resolution, TR/TE 832/34.6 ms, multi-band acceleration factor 6, 90 x 90 matrix, BW 2222 Hz/Px. Participants' responses were logged for further analyses.

4.3.2 Functional MRI Reward Magnitude Task

Adolescence is a critical developmental phase in the journey from childhood to adulthood, not only socially, behaviourally and physically, but also cognitively due to increased demands related to decision-making, valuation and motivation (Hartley and Somerville, 2015, Blakemore and Choudhury, 2006).

The Reward Magnitude task was developed as part of the Human Connectome in Development (HCP-D) study to assess neural circuits involved in reward processing. In the present study, the task was adapted for the South African setting by changing the currency to South African Rand. The task was programmed in PsychoPy2 software and displayed on a high-definition MR-compatible 32" Nordic Neurolab LCD screen that was viewed by participants using the standard mirror that mounts to the Siemens 32-channel head coil. Participants responded on a four-button Lumina response system using either their index or middle finger. Two-way communication between the participant, in the scanner, and the examiner, outside of the scanner, was possible through the built-in intercom. The participant was able to stop the scan at any time during the scanning procedure by squeezing a ball held in his/her non-dominant hand.

During the Reward Magnitude ("guessing") task (Figure 2), participants can win or lose money by guessing between two response options (baby – left button, adult – right button) whenever they see a question mark on the screen. For each trial, the *guess* cue ("?") is displayed for 1.5 seconds, followed by a jittered (1.5 - 2 s) interstimulus interval (ISI) during which a "+" is displayed, and then a *feedback* slide displayed for 1 second informing the participant whether they guessed correctly (winning money) or incorrectly (losing money). Trials are separated by a "+" that is similarly displayed for jittered timings (1.5 - 2 s). The task uses a block design. Each block of 4 trials is preceded by a "*stakes*" slide, displayed for 1.5 s, that informs the participant whether the next set of 4 trials will be played for high or low stakes, i.e., "low" magnitude outcomes or "high" magnitude outcomes. Participants are instructed that the computer will choose a response should they fail to respond to the "?" cue. Feedback is pre-programmed and is not linked to the participant's actual guess. As a result, participants receive the identical outcomes of their guesses and therefore the same monetary gains at the end of the task.

The Reward Magnitude Task aims to isolate neural responses during the anticipatory stakes period, the guessing period, and during each of the four feedback types: high win, high loss, low win, and low loss. General linear modeling permits analyses of 1) neural responses to receipt of reward or punishment, 2) differences in neural activity related to the magnitude of the reward or punishment (small vs large), and 3) neural activity in response to anticipation of high or low magnitude outcomes (Somerville et al., 2018).

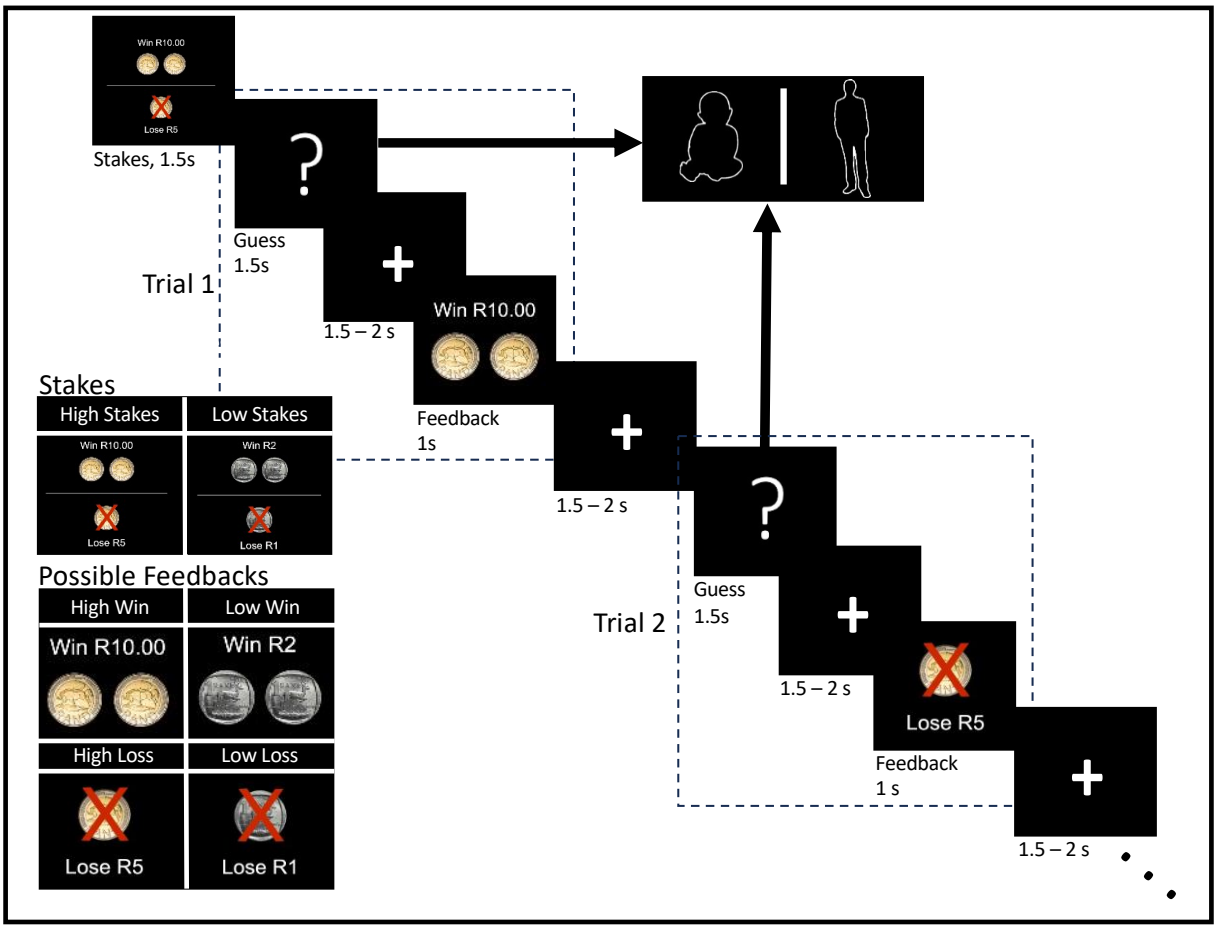

Figure 2: Illustration of the Reward Magnitude ("guessing") Task

4.3.3 Behavioural Analysis

The Reward Magnitude task takes 3 minutes, 35 seconds to complete. It comprises 6 blocks of 4 trials each. The blocks are presented in the following order: 1 low stakes, 2 high stakes, 1 low stakes, 1 high stakes, and 1 low stakes. Participants can therefore make a maximum of 24 guesses. All responses were logged together with the participants' response times. These data were used to assess the adolescents' participation in and engagement with the task.

4.3.4 Preprocessing

Preprocessing included skull stripping, motion artefact removal, and co-registration to the participant's high-resolution anatomical image. In this study, all preprocessing was done using fMRIPrep 21.0.1 (Esteban et al., 2019). It should be noted that fMRIPrep does not perform any

denoising (e.g., spatial smoothing). Details of the preprocessing pipeline are provided in Appendix A.

4.3.5 fMRI analysis

During first level analyses, performed using FSL FEAT (Woolrich et al., 2001), data were submitted to a Generalised Linear Model (GLM) to estimate task effects. The seven regressors included high stakes, low stakes, guess, high win, low win, high loss, and low loss. The GLM was solved for each voxel for each subject. The regressors of interest, mentioned previously, were represented as predictive timeseries by specifying their temporal event onsets, convolved with a double-gamma canonical hemodynamic response function. Motion estimates were included as predictors of no interest.

Group level analyses were also performed using FSL FEAT (Woolrich et al., 2004). Firstly, we investigated brain activation for the contrasts listed in Table 1 for the group as a whole to identify brain regions involved in reward processing and comparison with activations previously reported using the same task. Following this, we identified regions showing differences in brain activation for the same contrasts between CPHIV and controls, as well as between males and females, irrespective of HIV-status. Z-statistic images were thresholded at Z>3.1 and a cluster significance threshold of p=0.05. In the analysis of HIV-effects, we did not control for sex nor age, since the groups were well matched on sex and all children fell within a narrow age range.

Table 1: Summary of contrasts

	High stakes	Low stakes	High win	Low win	High loss	Low loss
H1: "Stakes" vs Rest	0.5	0.5	-	-	-	-
H2: Win vs Loss	-	-	0.5	0.5	-0.5	-0.5
H3a: High stakes vs Low stakes	0.5	-0.5	-	-	-	-
H3b: (High win - High loss) vs (Low win - Low loss)	-	-	0.5	-0.5	-0.5	0.5
H4a: High win vs Low win	-	-	0.5	-0.5	-	-
H4b: Low loss vs High loss	-	-	-	-	-0.5	0.5
H4c: Linear	-	-	0.75	0.25	-0.75	-0.25

Due to our interest in the current project on the processing of reward, our analyses focused on contrasts H1 ("stakes" vs rest), H2 (win vs loss) and H4a-c (high win vs low win; low loss vs high loss; linear association with increasing reward magnitude from high loss to high win). Contrast H3, which relates to effects of varying magnitudes on anticipation and reward processing, was not investigated further in this study.

Regions showing brain activation in the whole sample or group differences were labeled using *atlasquery* in FSL FEAT (Woolrich et al., 2004). *Atlasquery* gives the probability of a cluster being a member of the different labelled regions within the brain atlas. Since all the clusters identified in our study overlapped with multiple regions of the brain, no one anatomical label could be allocated to any cluster. In our results, we give probabilities as percentages next to each anatomical region. Only the anatomical regions with the largest percentages were used to describe the anatomical location of each cluster. In addition, we report MNI coordinates of the peak voxel in each cluster and cluster sizes.

Since contrast H2 encapsulates all wins vs all losses, irrespective of magnitude, we extracted BOLD percent signal change for each subject in regions showing group differences on this contrast to further interrogate how the different regressors contribute to the observed group differences. FeatQuery (Woolrich et al., 2001) was used to obtain the percent signal change in

these regions of interest (ROIs) for the relevant regressors (high win, low win, high loss, low loss) for each subject.

4.3.6 Post-hoc Statistical analyses

A two-sample one-tailed t-test was used to compare the mean % BOLD signal change for each of the 4 regressors of interest (high win, high loss, low win and low loss) between CPHIV and controls in regions showing group differences for win vs loss (H2). Pearson correlation was used to examine associations of age with the % signal change for the same regressors, as well as with the contrast win vs loss, in these regions.

5. Results

5.1 Sample Characteristics

We report results for 106 participants (66 CPHIV; mean age ± standard deviation 15±0.4 years; 45 males). The sample characteristics for the CPHIV and control groups are presented in Table 2.

In both the PHIV and control groups, only around 50% of children were in the expected school grade for their age (Government, 2022). This may be a consequence of the poor educational infrastructure typically seen in communities of low socioeconomic status (Hall, et. al., 2019). The TANNER scores (WHO, 2010) for both CPHIV and controls were around 4, indicating that children had mostly reached puberty. Since groups were matched on age, sex and home language, these were not controlled for in our analyses.

It should also be noted that no subjects in this study had high viral loads. Viral loads were suppressed in 95% of the CPHIV.

Although groups were well matched on sex and TANNER scores (*p's* > 0.261), CPHIV were about 4 months younger on average (two-tailed independent sample student's t-test, $p = 0.02$) and slightly smaller (in terms of weight and height) than controls (*p*'s = 0.0046 and 0.0003, respectively). Home language also tended to differ between groups (chi square $p = 0.065$), with fewer Afrikaans-speaking and more Xhosa-speaking adolescents in the CPHIV than control group. However, it is important to note that the Reward Magnitude Task was explained in the participant's home language and practiced before commencing the scan.

Table 2: Sample Characteristics

Demographics:	CPHIV	Controls
Sample Size (N)	66	40
Age at scan (years, mean±sd)	14.93±0.35	15.27±0.46
Males (% males)	27 (40.9%)	18 (45.0%)
Weight at scan (kg, mean±sd)	52.06±11.97	60.39±15.13
Height at scan (cm, mean±sd)	154.68±7.49	161.29±9.11
School Grade: [1]		
6	1 (1.64%)	0
7	11 (18.03%)	8 (20.51%)
8	17 (27.87%)	8 (20.51%)
9	26 (42.62%)	22 (56.41%)
10	6 (9.84%)	1 (2.56%)
Correct school grade for age (n, %) [2]	32 (52.46%)	19 (48.72%)
Lower grade than expected for age (n, %)	27 (44.26%)	18 (46.15%)
TANNER Score [3]	4.09±0.83	3.88±0.78
Home Language:		
Afrikaans	8 (12%)	11 (27.5%)
English	1 (1.5%)	2 (5%)
Xhosa	57 (86.4%)	27 (67.5%)
Clinical data at enrollment:[4]		
CD4 Count (cells/mm³, mean±sd)	1667.49±889.59	-
CD4% (mean±sd)	31.46±10.72	-
Viral Load		
High (>750,000 copies/mL)	39 (60%)	-
Low (400-750,000 copies/mL)	26 (40%)	-
Suppressed (<400 copies/mL)	0	-
Clinical data at scan:		

CD4 Count (cells/mm³, mean±sd) [5]	812.06±239.86	-
CD4% (mean±sd) [5]	37.23±6.75	-
Viral Load [6]		
High (>750,000 copies/mL)	0	-
Low (400-750,000 copies/mL)	3 (4.55%)	-
Suppressed (<400 copies/mL)	63 (95.45%)	-

sd = standard deviation

[1]Data only included for the 100 adolescents (61 CPHIV, 39 Controls) who attend schools within the South African Government school system; remaining participants attend Schools of Skills, which are not directly comparable.

[2]For each child, their recorded school grade was compared to the expected school grade for age. 2 CPHIV and 2 controls were excluded due to being in a higher grade.

[3]Indication of puberty. 2 measurements for each sex, i.e., females = pubic hair growth + breast development; males = pubic hair growth + genitalia development. Each measurement is given a score out of 5, with 1 being no sign of onset (prepubertal) and 5 being total onset (total pubertal). The total score is divided by 2 to obtain a TANNER score out of 5. CPHIV=46, Controls=33. Tanner data acquired within 6 months of the scan.

[4]Enrollment data available for 65 CPHIV: all 57 CHER CPHIV (enrollment age 6-12 weeks), and 8 IMPAACT CPHIV (enrollment age 22-88 weeks). 1 IMPAACT participant's data could not be found.

[5]CD4 data available for 53 CPHIV, CD4 data of remaining participants not acquired; clinical data acquired within 1 year of scan.

[6]Viral load data for all 66 CPHIV; clinical data acquired within 1 year of scan.

5.2 Behavioural Data

Table 3 summarises the task behavioural data for CPHIV and controls, including the number of responses and response times (RT). Due to a faulty response box, and one participant who did not press any buttons, we only report RT data for 92 of the 106 participants included in the fMRI analysis. No participants were excluded from the fMRI analyses due to incomplete or missing behavioural data.

RTs are given for all trials combined, and for high- and low-stakes trials separately. Notably, RTs for low-stakes trials were not significantly faster than for high-stakes trials in either group (CPHIV: 1-tailed t-test p= 0.386; controls: p= 0.327). However, for CPHIV, the RTs across all trials were significantly faster than for controls. When examined separately, CPHIV responded faster than controls on both high- and low-stakes trials, although the reduction in RT was below conventional levels of significance for low-stakes trials. The guesses of twenty-four children (14 CPHIV) did not include both options (baby and adult). Choosing only one of the two possible responses (i.e., baby or adult) might be a strategy by these participants as it ensures a 50% chance of being right. The average response times for these participants are also shown.

Table 3: Behavioural Data - Task Participation

All types of responses*	**CPHIV (N = 63)**	**Controls (N = 29)**	***p*-value[1]**
Number of responses (median; [IQR])	22 [19, 24]	21 [13, 23]	0.08
RT (s, mean $\pm$ sd)	0.76 $\pm$ 0.18	0.84 $\pm$ 0.20	0.03
High Stakes RT (s, mean $\pm$ sd)**	0.77 $\pm$ 0.19	0.85 $\pm$ 0.23	0.05
Low Stakes RT (s, mean $\pm$ sd)**	0.76 $\pm$ 0.20	0.83 $\pm$ 0.21	0.08
Number of participants that pressed the same button throughout the task***	**CPHIV (N = 14)**	**Controls (N = 10)**	
RT (s, mean $\pm$ sd)	0.70 $\pm$ 0.23	0.83 $\pm$ 0.24	0.11

RT = Response Time (s); sd = standard deviation; [1]1-tailed student's t-test

*Due to a faulty response button, and 1 participant not pressing any buttons, responses of only 92 participants were correctly logged.

**One participant who had no responses during the high-stakes blocks was excluded; another participant who had no responses during the low-stakes blocks was excluded.

***Only includes participants who provided a valid response (1 choice).

5.3 Functional MRI Results

5.3.1 fMRI analysis

As mentioned earlier, due to the focus of our project being the processing of reward and the impact of different reward magnitudes, our analyses focused on contrasts H1, H2 and H4a-c in Table 1. Contrast H1 ("stakes" vs rest) provides insight into anticipation for reward or loss, since the stakes for a subsequent block of 4 trials is given before the trials commence. Contrast H2 (win>loss) addresses the aim of this study, which is to examine whether living with HIV alters brain activity during processing of reward (win) compared to punishment (loss). While contrasts H3a and b interrogate the effect of magnitude on anticipation (high vs low stakes) and processing of reward vs punishment (high vs low), respectively, contrasts H4a-b provide insight into differences in brain activation due to high vs low wins, and high vs low losses. Contrast H4c allows identification of brain regions showing increasing activation or deactivation with increasing reward magnitude, from high loss to high win.

In the sections below, we present for each contrast first brain regions activated by the whole sample, and then regions showing group differences for that contrast. Notably, for all contrasts investigated, controls activated regions very similar to those activated by the whole sample, and no regions were identified where CPHIV showed greater activation than controls.

a. Anticipation of reward or loss (H1: "stakes" vs rest)

Figure 3 and Table 4 respectively show and list brain regions activated in the whole sample during anticipation of reward or loss. Notably, large bilateral activations were seen in occipital cortices, middle frontal and precentral gyri, insula and cerebellar cortices, medial paracingulate and cingulate cortices, vermis, left frontal pole, and left middle and superior temporal gyri. Activation of left temporal regions may point to language involvement, possibly to verbalise the magnitude of the stakes being played for.

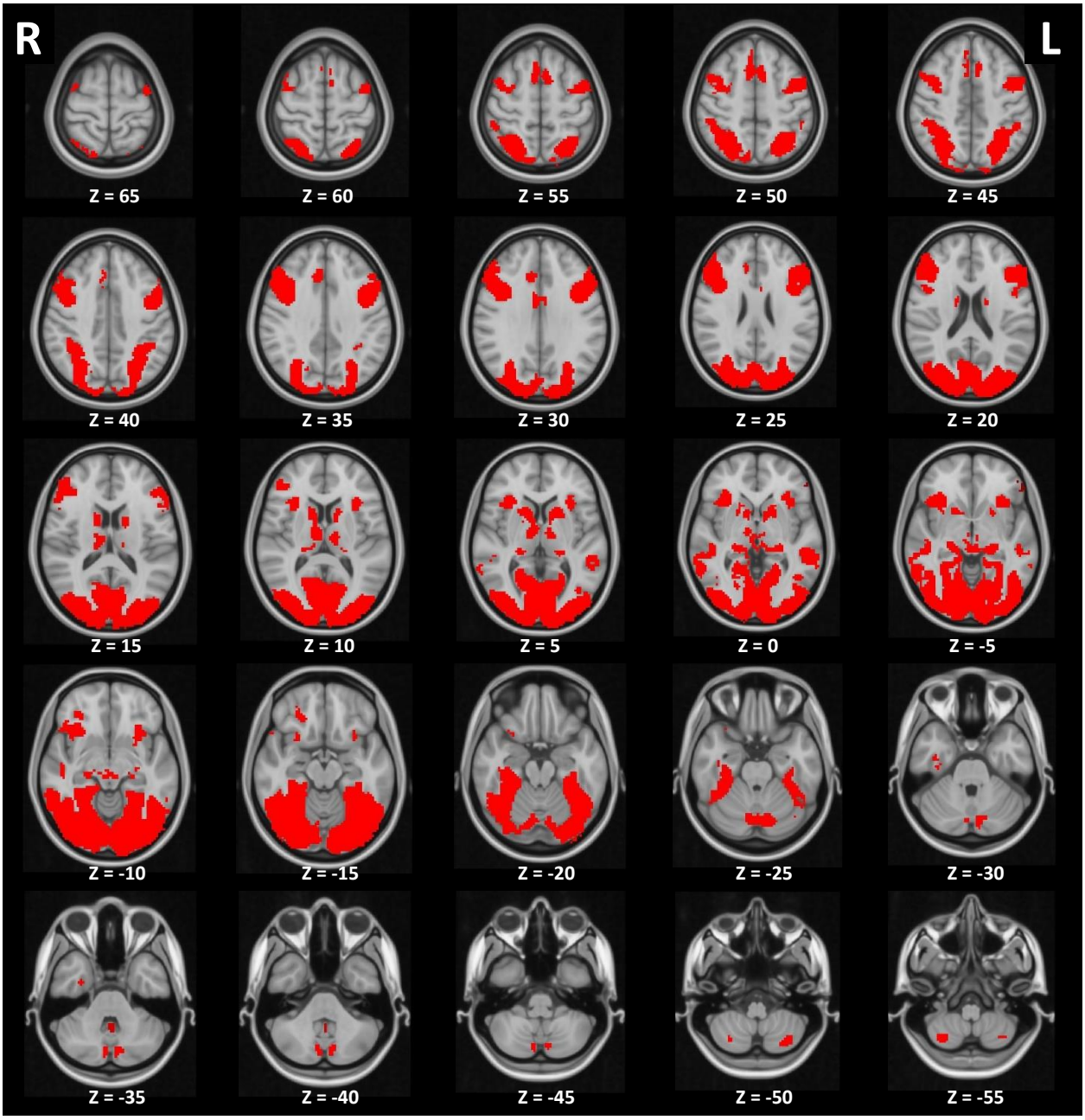

Figure 3: Axial slices showing brain regions activated by the whole sample during anticipation of reward or loss (i.e., "stakes" vs rest); R = Right; L = Left; Z>3.1 and a cluster significance threshold of p=0.05

Table 4: Brain regions activated during "stakes" vs rest in all children (contrast H1)

	Anatomical region	**Peak X, Y, Z (MNI, mm) & cluster size (mm^3)**	**Illustration of cluster location**
1.	Lateral Occipital Cortex, superior division: 9% Lateral Occipital Cortex, inferior division: 6% Lingual Gyrus: 6% Occipital Pole: 9%	(-26.9; -62.9; -8.9) 249,717	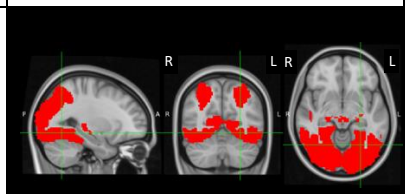
2.	Right Middle Frontal Gyrus: 22% Right Precentral Gyrus: 10%	(35.5; 9.1; 31.9) 23,086	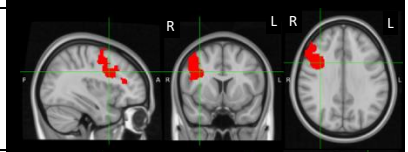
3.	Left Middle Frontal Gyrus: 19% Left Precentral Gyrus: 17%	(-41.3; -0.5; 36.7) 20,017	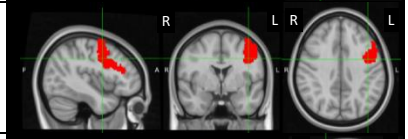
4.	Right Insular Cortex: 16%	(33.1; 18.7; -4.1) 7,782	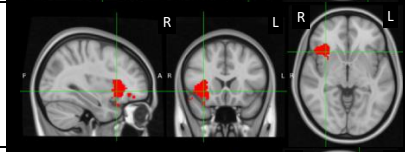
5.	Left Insular Cortex: 14%	(-29.3; 18.7; -6.5) 6,718	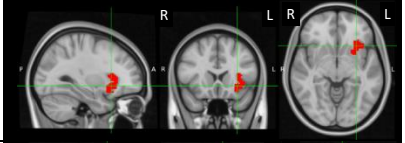
6.	Superior Frontal Gyrus: 16% Paracingulate Gyrus: 29%	(-5.3; 11.5; 53.5) 6,649	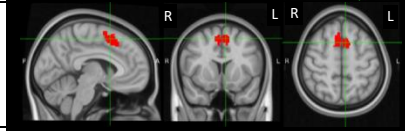
7.	Left Superior Temporal Gyrus, posterior division: 24% Left Middle Temporal Gyrus, posterior division: 20%	(-55.7; -41.3; 0.7) 3,027	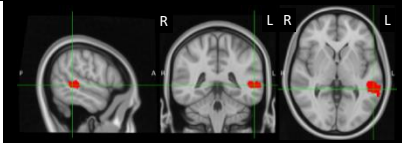
8.	Left Crus II: 44% Left VIIb: 50%	(-29.3; -72.5; -49.7) 815	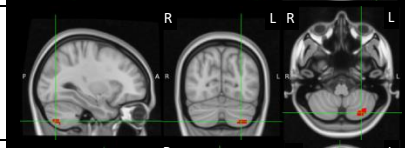
9.	Cingulate Gyrus, anterior division: 40%	(4.3; 1.9; 29.5) 801	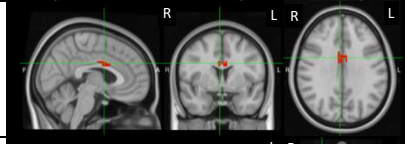
10.	Right VIIb: 59% Right VIIIa: 33%	(30.7; -65.3; -54.5) 608	

11.	Vermis IX: 44% Vermis X: 21%	(-0.5; -50.9; -35.3) 414	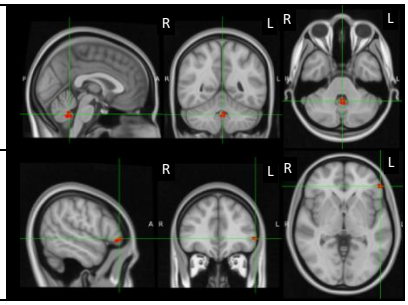
12.	Left Frontal Pole: 36% Left Inferior Frontal Gyrus, pars triangularis: 21%	(-53.3; 37.9; -1.7) 304	

R, Right; L, Left; Z>3.1 and a cluster significance threshold of *p*=0.05

When comparing CPHIV and controls, we identified three regions where CPHIV showed less activation during anticipation of reward or loss compared to controls (Table 5), namely the left occipital pole, left temporal pole / orbitofrontal cortex, and paracingulate / anterior cingulate gyrus.

No differences were seen between males and females in the processing of anticipation.

Table 5: Regions where CPHIV demonstrated smaller activation increases during anticipation of reward or loss ("stakes" vs rest) than controls (H1)

	Anatomical region	**Peak X, Y, Z (MNI, mm) & cluster size (mm^3)**	**Illustration of cluster location**
1.	L Occipital Pole: 52%	(-17.3; -101; 3.1) 857	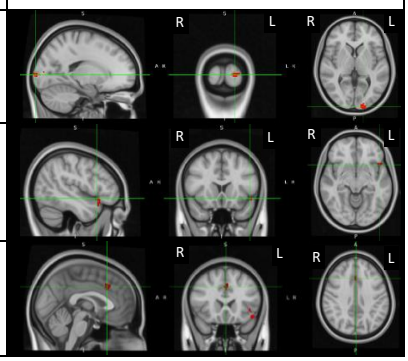
2.	L Temporal Pole: 18% L Frontal Orbital Cortex: 28%	(-46.1; 16.3; -8.9) 318	
3.	Paracingulate Gyrus: 57% Cingulate Gyrus, anterior division: 22%	(-0.5; 21.1; 36.7) 304	

R, Right; L, Left; Z>3.1 and a cluster significance threshold of *p*=0.05

b. **Processing of reward vs punishment (H2: win vs loss)**

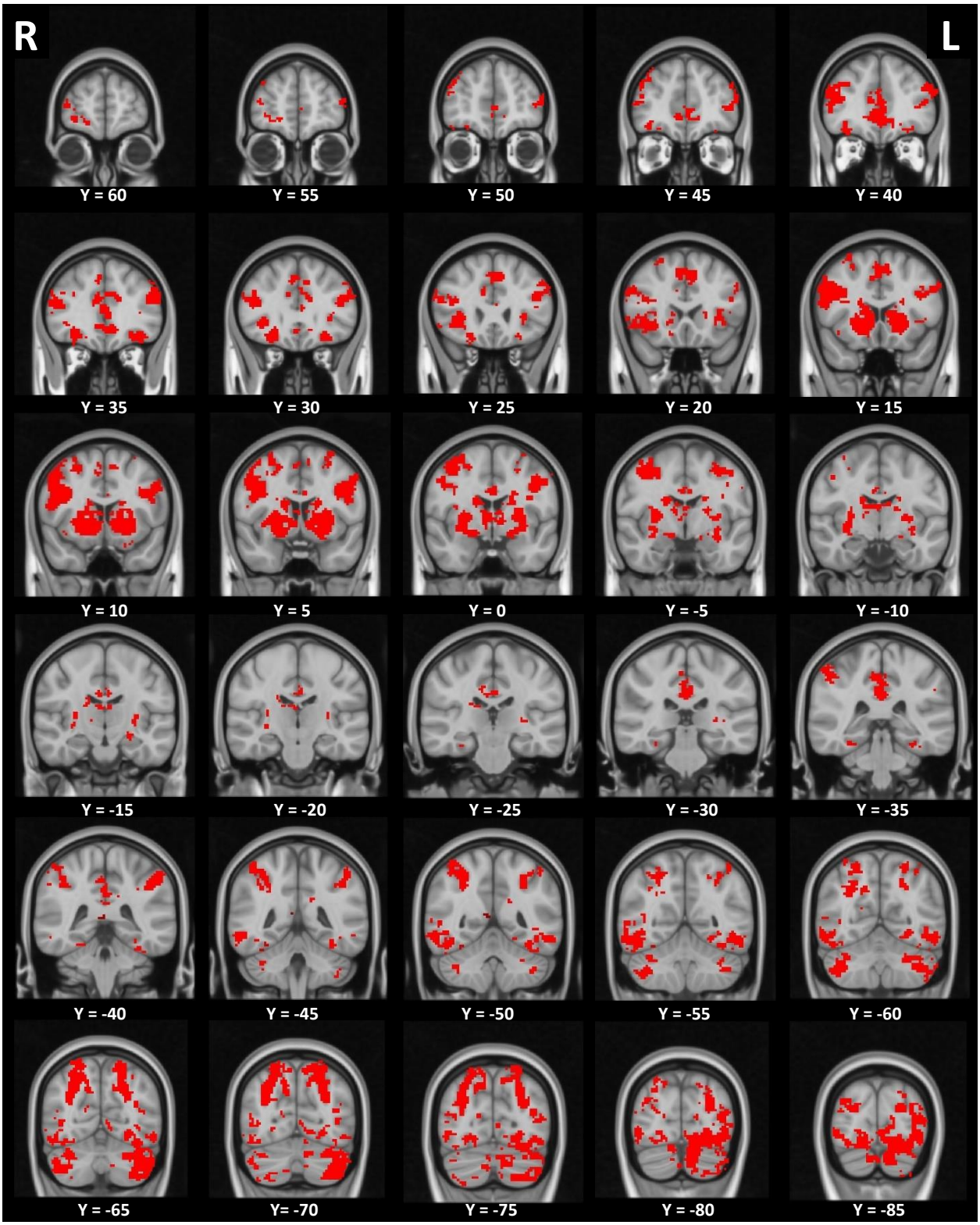

Figure 4: Coronal slices showing brain regions activated more during reward than punishment ("win" vs "loss") by the whole sample; R = Right; L = Left; Z>3.1 and a cluster significance threshold of p=0.05

Table 6: Brain regions showing greater activation in the whole sample during processing of reward compared to punishment (contrast H2, "win" vs "loss")

	Anatomical region	**Peak X, Y, Z (MNI, mm) & cluster size (mm^3)**	**Illustration of cluster location**
1.	L + R Lateral Occipital Cortex, superior division: 14% L + R Occipital Pole: 11%	(-12.5; -96.5; 3.1) 96,353	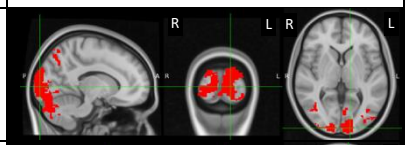
2.	L + R Cerebral White Matter: 29% R Cerebral Cortex: 14% L + R Putamen: 23%	(-10.1; 9.1; 0.7) 38,610	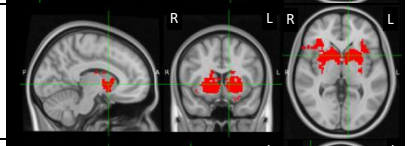
3.	R Middle Frontal Gyrus: 15% R Precentral Gyrus: 15% R Frontal Pole: 10%	(47.5; 9.1; 22.3) 22,160	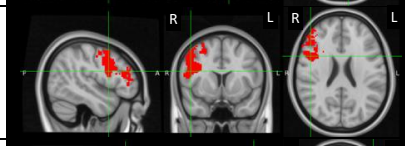
4.	L Middle Frontal Gyrus: 16% L Precentral Gyrus: 16% L Frontal Pole: 8%	(-48.5; 35.5; 27.1) 13,299	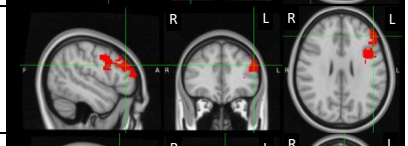
5.	L + R Paracingulate Gyrus: 33% L + R Cingulate Gyrus, anterior division: 25%	(-5.3; 25.9; 41.5) 11,280	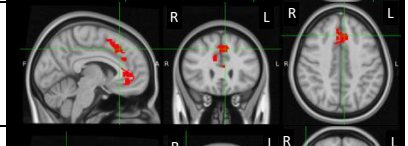
6.	R Middle and Inferior Temporal Gyrus, temporo-occipital part: 37% R Inferior Lateral Occipital Cortex: 14%	(54.7; -55.7; -13.7) 6,843	
7.	L + R Cingulate Gyrus, anterior and posterior division: 54%	(-2.9; -31.7; 29.5) 5,668	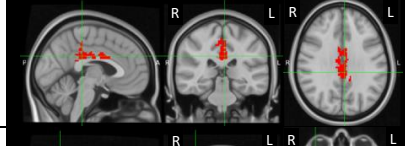
8.	R Crus I: 52% R Crus II: 24%	(40.3; -65.3; -42.5) 4,949	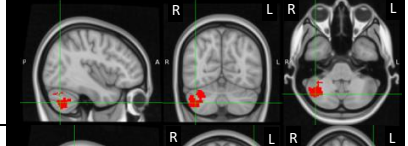
9.	L Superior Parietal Lobule: 16% L Supramarginal Gyrus, anterior and posterior division: 31%	(-48.5; -43.7; 51.1) 4,285	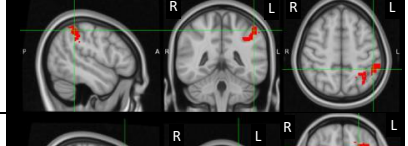
10.	L Frontal Pole: 32% L Orbital Frontal Cortex: 41%	(-24.5; 33.1; -13.7) 1,576	
11.	R Frontal Pole: 52%	(28.3; 57.1; -8.9) 829	

12.	R Crus II: 27% R VIIb: 54%	(25.9; -67.7; -47.3) 788	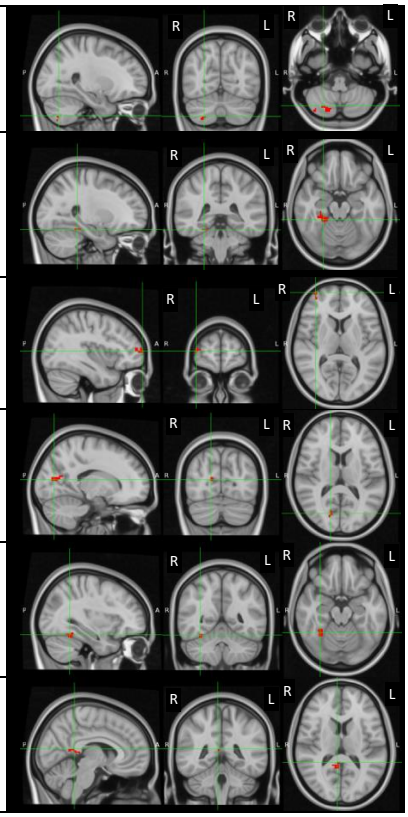
13.	R Parahippocampal Gyrus, posterior division: 29% R Temporal Fusiform Cortex, posterior division: 31%	(25.9; -38.9; -18.5) 415	
14.	R Frontal Pole: 68%	(37.9; 61.9; 7.9) 415	
15.	R Intracalcarine Cortex: 31%	(16.3; -74.9; 12.7) 346	
16.	R Temporal Occipital Fusiform Cortex: 65%	(33.1; -50.9; -18.5) 332	
17.	R Cingulate Gyrus, posterior division: 21% R Precuneus Cortex: 13%	(6.7; -43.7; 12.7) 332	

R, Right; L, Left; Z>3.1 and a cluster significance threshold of *p*=0.05

Across all subjects, there were robust activation to win>loss in bilateral occipital cortices, frontal poles / orbitofrontal cortices, striatum, and middle frontal and precentral gyri, medial paracingulate and cingulate gyri, right (R) cerebellar, precuneus, fusiform & intracalcarine cortices, and left (L) supramarginal gyrus / superior parietal lobule (Figure 4 and Table 6). Males and females showed no differences for the contrast win>loss. However, when comparing CPHIV and controls, CPHIV showed smaller activation increases for wins than losses compared to controls in a small cluster in the left superior and middle frontal gyrus (Table 7).

Table 7: Regions where activation increases for wins compared to losses were smaller in CPHIV than controls (contrast H2)

	Anatomical region	**Peak X, Y, Z (MNI, mm) & cluster size (mm^3)**	**Illustration of cluster location**
1.	L Superior and Middle Frontal Gyrus: 36 %	(-19.7; 25.9; 39.1) 332	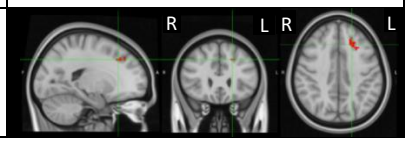

R, Right; L, Left; Z>3.1 and a cluster significance threshold of *p*=0.05

c. Magnitude of Reward (H4a: high win vs low win)

When comparing high and low wins in the whole sample, we found greater activation during high wins bilaterally in the occipital, fusiform, insular and intracalcarine cortices, and pre- and postcentral gyri, the right inferior, middle and superior temporal gyri, right middle frontal / precentral gyrus, left cerebellar cortex, and a medial posterior cingulate / precuneus region (Figure 5 and Table 8).

We did not find any regions where activation increases during high wins compared to low wins differed in CPHIV compared to controls, nor between males and females.

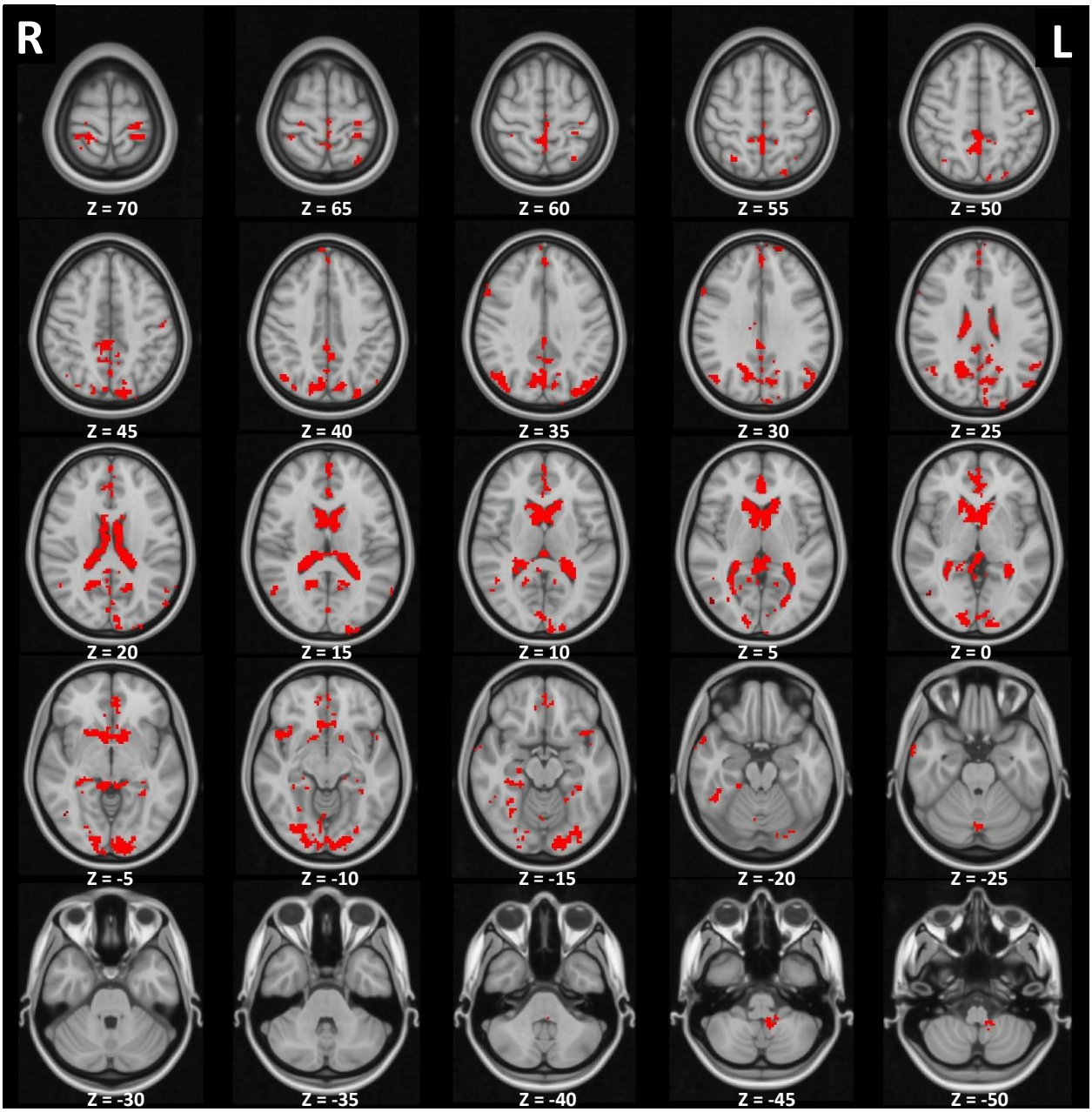

Figure 5: Axial slices showing brain regions activated more during high wins than low wins in the whole sample; R = Right; L = Left; Z>3.1 and a cluster significance threshold of p=0.05

Table 8: Brain regions showing greater activation during high wins than low wins in all children (contrast H4a)

	Anatomical region	**Peak X, Y, Z (MNI, mm) & cluster size (mm^3)**	**Illustration of cluster location**
1.	L + R Cerebral White Matter: 25% L + R Cerebral Cortex: 31%	(-24.5; -46.1; 15.1) 48,757	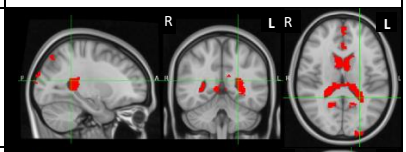
2.	Occipital Fusiform Gyrus: 18% Occipital Pole: 24%	(-17.3; -89.3; -11.3) 10,617	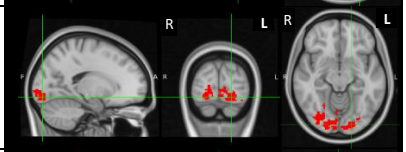
3.	Cingulate Gyrus, posterior division: 25% Precuneus Cortex: 33%	(1.9; -38.9; 48.7) 6,138	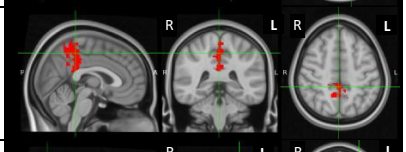
4.	L Lateral Occipital Cortex, superior division: 59%	(-29.3; -82.1; 36.7) 2,903	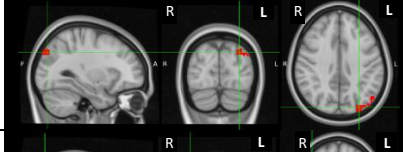
5.	R Lateral Occipital Cortex, superior division: 56%	(40.3; -77.3; 34.3) 2,626	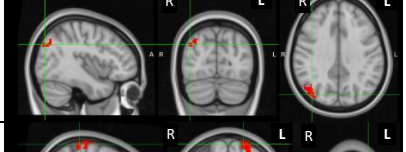
6.	L Precentral Gyrus: 16% L Postcentral Gyrus: 24%	(-22.1; -36.5; 75.1) 2,447	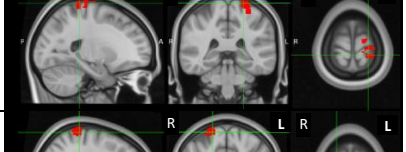
7.	R Postcentral Gyrus: 31%	(21.1; -36.5; 72.7) 1,479	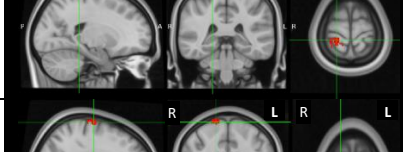
8.	R Precentral Gyrus: 33% R Postcentral Gyrus: 7%	(18.7; -14.9; 75.1) 816	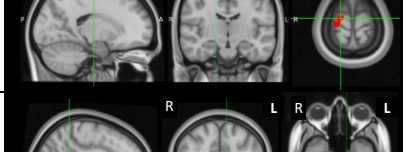
9.	Left IX: 50%	(-10.1; -48.5; -44.9) 677	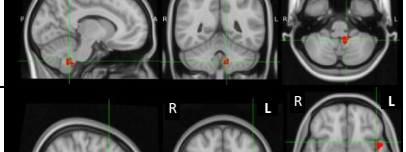
10.	L Insular Cortex: 6% L Temporal Pole: 30%	(-43.7; 13.9; -11.3) 677	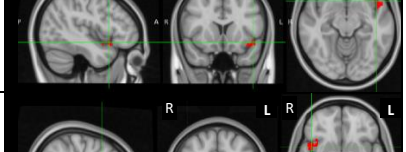
11.	R Insular Cortex: 33% R Temporal Pole: 16%	(45.1; 11.5; -8.9) 664	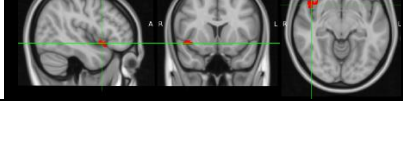

12.	R Temporal Pole: 27% R Superior and Middle Temporal Gyrus, anterior division: 32%	(66.7; -0.5; -13.7) 622	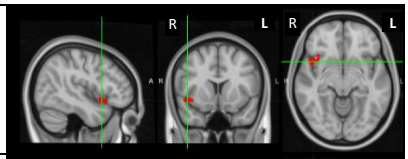
13.	R Inferior Temporal Gyrus, temporooccipital part: 27% R Temporal Occipital Fusiform Cortex: 41%	(45.1; -48.5; -18.5) 525	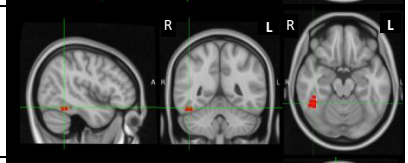
14.	Intracalcarine Cortex: 14% Supracalcarine Cortex: 29% Occipital Pole: 14%	(6.7; -84.5; 10.3) 511	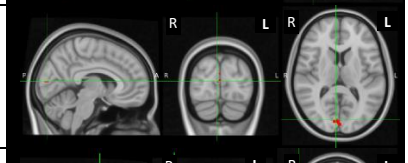
15.	R Middle Frontal Gyrus: 12% R Precentral Gyrus: 9%	(57.1; 16.3; 34.3) 401	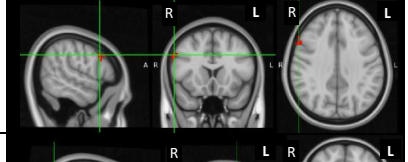
16.	L Intracalcarine Cortex: 18%	(-19.7; -74.9; 5.5) 401	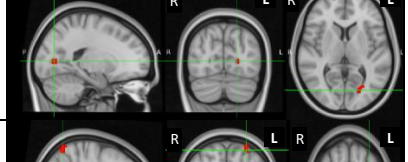
17.	L Lateral Occipital Cortex, superior division: 38%	(-29.3; -62.9; 60.7) 387	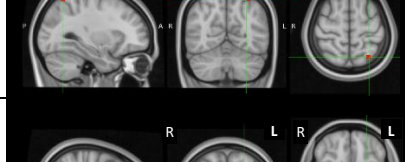
18.	L Lingual Gyrus: 13% L Temporal Fusiform Cortex, posterior division: 12% L Temporal Occipital Fusiform Cortex: 40%	(-24.5; -55.7; -13.7) 387	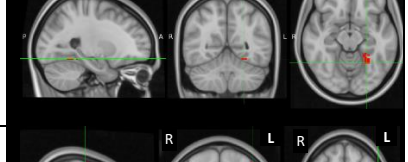
19.	L Precentral Gyrus: 24% L Postcentral Gyrus: 43%	(-48.5; -14.9; 48.7) 359	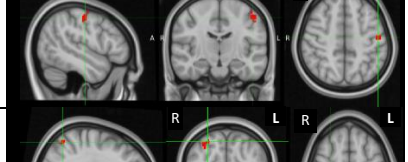
20.	R Lateral Occipital Cortex, superior division: 57%	(28.3; -62.9; 55.9) 332	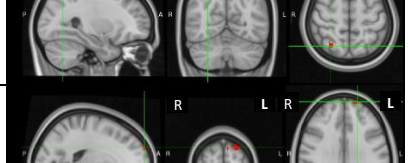
21.	Frontal Pole: 51%	(-19.7; 61.9; 29.5) 318	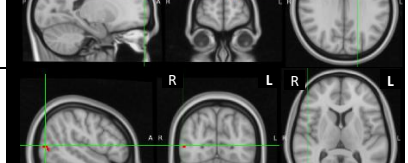
22.	R Lateral Occipital Cortex, inferior division: 63%	(49.9; -72.5; 7.9) 304	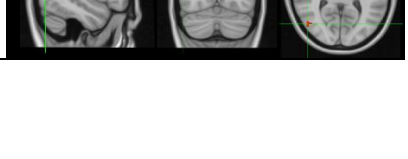

R, Right; L, Left; Z>3.1 and a cluster significance threshold of *p*=0.05

d. Magnitude of Loss (H4b: low loss vs high loss)

Contrast H4b compares activation between high and low losses. We found no activation differences between high and low losses within the group as a whole, nor within CPHIV and controls separately. This finding suggests that adolescents process large and small losses similarly.

We also did not find any regions where activation differences between high and low losses differed between CPHIV and controls, nor between males and females.

e. Linear association with increasing reward magnitude (H4c)

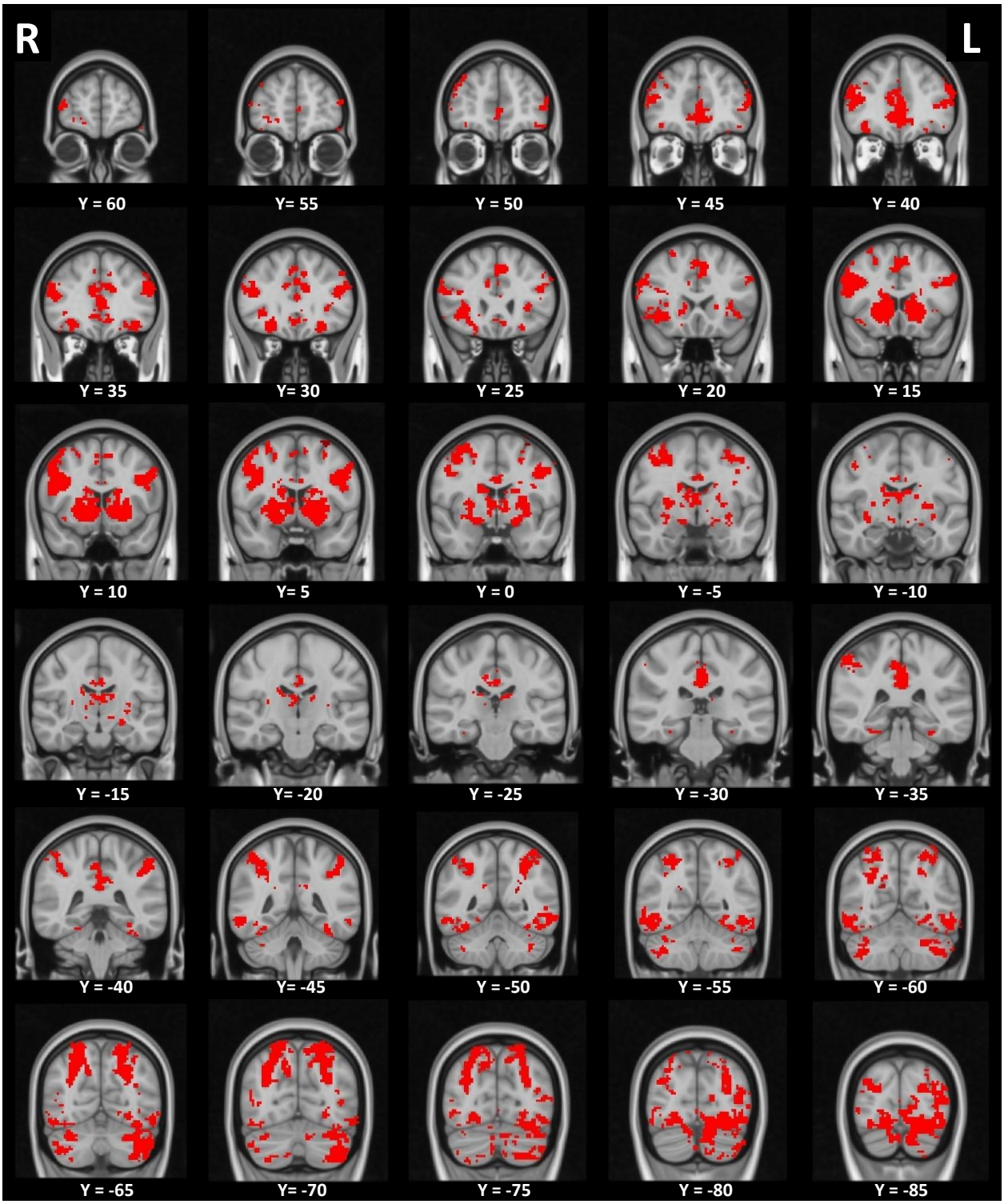

Figure 6: Coronal slices showing brain regions that exhibit increasing activation with increasing reward magnitude in the whole sample; R = Right; L = Left; Z>3.1 and a cluster significance threshold of p=0.05

Table 9: Brain regions showing increasing activation with increasing reward magnitude in all children (contrast H4c)

	Anatomical region	**Peak X, Y, Z (MNI, mm) & cluster size (mm^3)**	**Illustration of cluster location**
1.	Occipital Pole: 10%	(16.3; -94.1; 5.5) 111,684	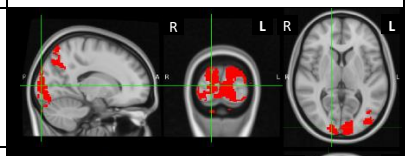
2.	L + R Cerebral White Matter: 28% L + R Putamen: 22% R Cerebral Cortex: 13% R Caudate: 7%	(21.1; 4.3; -8.9) 37,574	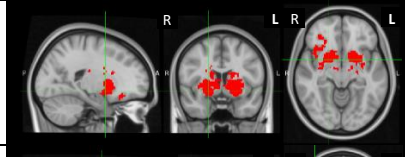
3.	R Frontal Pole: 11% R Middle Frontal Gyrus: 15% R Precentral Gyrus: 15%	(42.7; 9.1; 27.1) 20,238	
4.	Paracingulate Gyrus: 34% Cingulate Gyrus, anterior division: 27%	(-2.9; 37.9; 7.9) 13,879	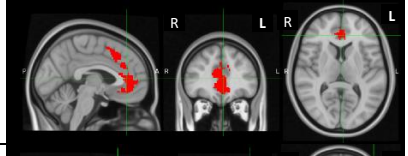
5.	L Frontal Pole: 10% L Middle Frontal Gyrus: 16% L Precentral Gyrus: 15%	(-48.5; 35.5; 24.7) 11,211	
6.	Cingulate Gyrus, anterior division: 10% Cingulate Gyrus, posterior division: 45%	(-2.9; -31.7; 29.5) 7,161	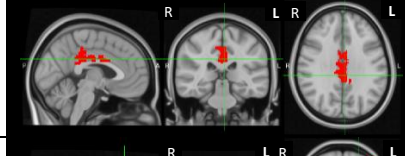
7.	L Frontal Pole: 33% L Frontal Orbital Cortex: 36%	(-24.5; 33.1; -13.7) 1,922	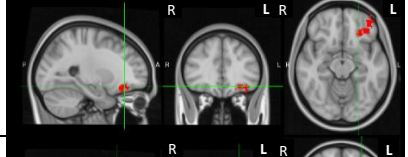
8.	L Insular Cortex: 28% L Frontal Orbital Cortex: 10%	(-29.3; 28.3; 3.1) 1,396	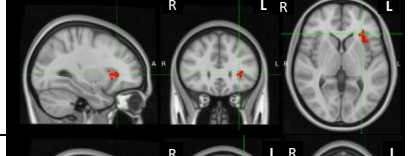
9.	L Middle Frontal Gyrus: 18% L Precentral Gyrus: 29%	(-31.7; -5.3; 53.5) 1,299	
10.	R Crus II: 26% R VIIb: 46% R VIIIa: 9%	(30.7; -74.9; -52.1) 1,078	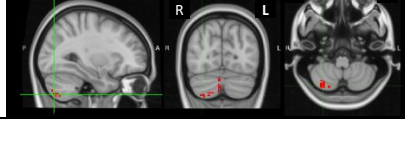

11.	R Superior Frontal Gyrus: 26% R Middle Frontal Gyrus: 23%	(25.9; 18.7; 58.3) 691	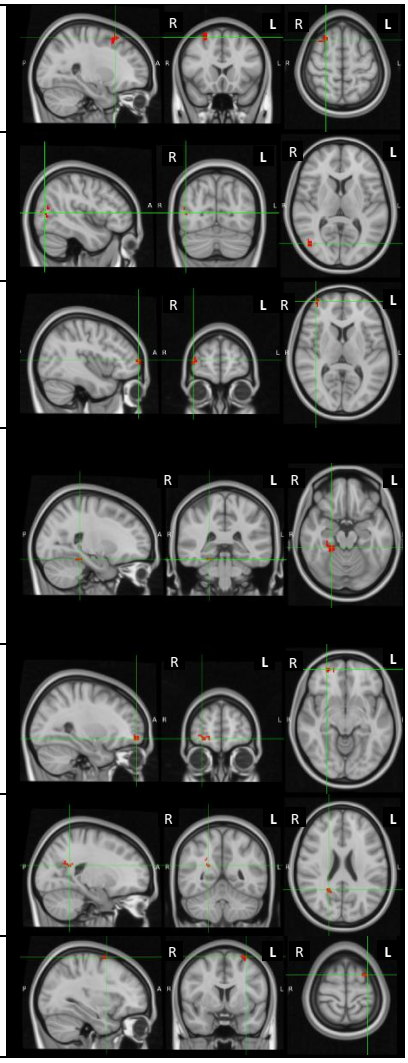
12.	R Lateral Occipital Cortex, superior division: 12% R Lateral Occipital Cortex, inferior division: 41%	(45.1; -72.5; 7.9) 567	
13.	R Frontal Pole: 62%	(40.3; 59.5; 7.9) 387	
14.	R Parahippocampal Gyrus, posterior division: 32% R Temporal Fusiform Cortex, posterior division: 26% R Temporal Occipital Fusiform Cortex: 14%	(23.5; -36.5; -18.5) 345	
15.	R Frontal Pole: 51%	(28.3; 57.1; -8.9) 332	
16.	R Precuneus Cortex: 25%	(21.1; -50.9; 22.3) 318	
17.	L Superior Frontal Gyrus: 16% L Middle Frontal Gyrus: 20%	(-31.7; 4.3; 67.9) 318	

R, Right; L, Left; Z>3.1 and a cluster significance threshold of p=0.05

Figure 6 and Table 9 respectively show and list brain regions showing increasing activation (or deactivation) with increasing reward magnitude. Similar to activations seen when comparing reward vs punishment (contrast H2), increasing reward was associated with increasing activation bilaterally in the occipital and orbitofrontal cortices, striatum, precentral gyrus, and superior and middle frontal gyri, medially in the paracingulate and cingulate gyri, and R cerebellar, precuneus and fusiform cortices. In addition, we observed increasing activation in the L insula, not seen in contrast H2. We did not observe increasing activation in the L supramarginal gyrus / superior parietal lobule region seen in the H2 contrast.

When comparing groups, CPHIV demonstrated smaller activation increases than controls in 3 frontal clusters – two adjacent clusters in the left superior and middle frontal region and another in the left paracingulate gyrus (Table 10). No regions demonstrated differences between males and females.

Table 10: Regions where activation increases with increasing reward magnitude are smaller in CPHIV than controls (H4c)

	Anatomical region	**Peak X, Y, Z (MNI, mm) & cluster size (mm^3)**	**Illustration of cluster location**
1.	L Superior Frontal Gyrus: 20% L Middle Frontal Gyrus: 21%	(-24.5; 28.3; 39.1) 622	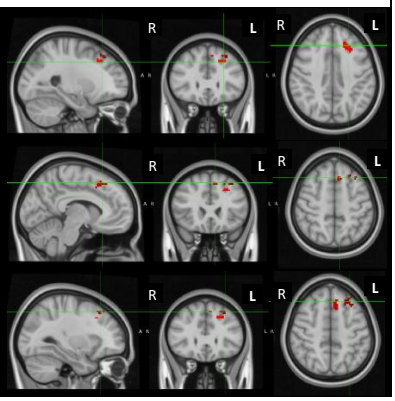
2.	L Superior Frontal Gyrus: 20% L Paracingulate Gyrus: 13%	(-7.7; 23.5; 51.1) 456	
3.	L Superior Frontal Gyrus: 22% L Middle Frontal Gyrus: 34%	(-29.3; 28.3; 48.7) 456	

R, Right; L, Left; Z>3.1 and a cluster significance threshold of p=0.05

5.3.2 Post-hoc Statistical analyses

Table 11 summarizes the group means of the % BOLD signal change for each condition (high win, high loss, low win, low loss, win>loss) in the small left frontal cluster where CPHIV demonstrated smaller activation increases for wins compared to losses than controls (Table 7). Our post-hoc analyses reveal that the group difference seen in the win>loss contrast is largely attributable to the absence of activation increases in this region during high wins in the CPHIV. BOLD % signal changes during loss conditions were similar between groups (all p's > 0.4). In contrast to controls who showed greater activation increases for high than low wins (one-tailed paired t-test, p=0.007), BOLD signal changes for high and low wins were similar in CPHIV (p=0.3) (Figure 7).

Finally, the association of increasing age with greater activation increases for wins compared to losses, appear to be attributable to age-related decreases in activation (albeit weakly and only at

a trend level) during high loss conditions. Percent BOLD signal change during high wins, low wins and low loss did not show any association with age (all *p*'s > 0.27).

Table 11: Group comparison of the % BOLD signal change for each condition and associations with age

	Mean % BOLD signal change ± Standard Deviation		1-tailed t-test *p*-value	Pearson Correlation with age
	CPHIV (*N* = 66)	Controls (*N* = 40)	CPHIV vs controls	*r* (*p*)
High Win	-0.12 ± 0.22	0.05 ± 0.24	**0.0002**	0.015 (0.875)
High Loss	-0.08 ± 0.26	-0.09 ± 0.24	0.469	-0.158 (0.106)
Low Win	-0.14 ± 0.23	-0.07 ± 0.24	0.074	0.107 (0.277)
Low Loss	-0.11 ± 0.22	-0.12 ± 0.25	0.396	-0.018 (0.854)
Win>Loss	-0.05 ± 0.19	0.11 ± 0.19	**0.00003**	0.220 (0.024)

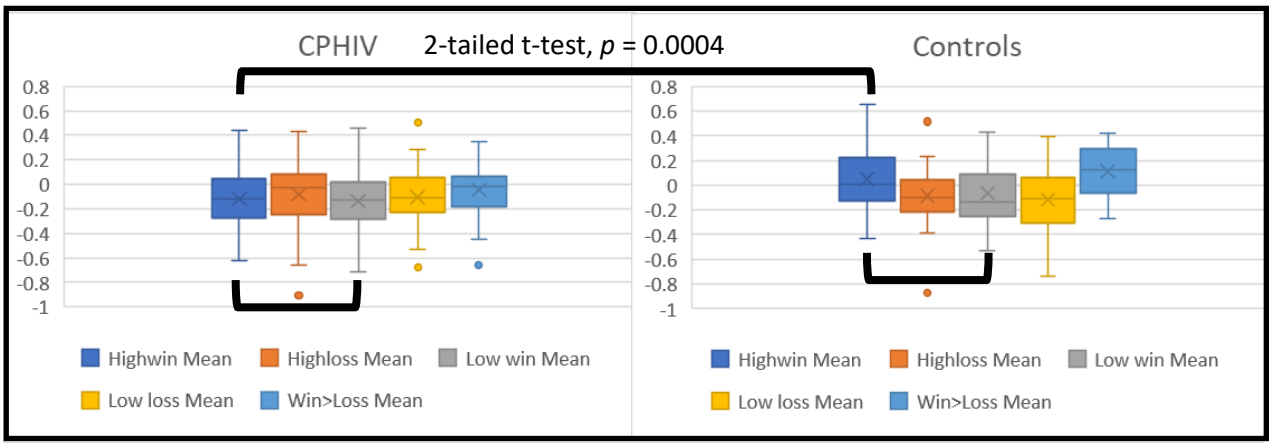

Figure 7: Box plots indicating % BOLD signal change for each condition in the left superior frontal cluster where CPHIV showed smaller activation increases compared to controls for wins than losses

To validate our finding of greater activation in controls than CPHIV in this region during high wins, we conducted a voxel-wise group comparison for the high win vs rest contrast. Our analyses

revealed a cluster (shown in Figure 8) that overlaps directly with that shown in the figure of table 7, where controls showed greater activation during high wins than CPHIV.

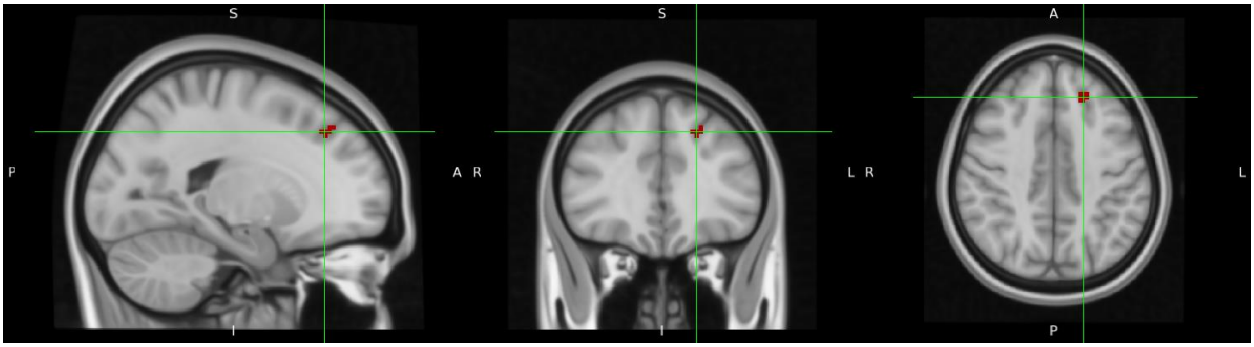

Figure 8: Left superior and middle frontal cluster where CPHIV show less activation than controls during the high win condition (size: 415 mm3; peak MNI coordinates: -19.7; 33.1; 41.5); R, Right; L, Left; Z>3.1 and a cluster significance threshold of p=0.05

Given that group differences in reward processing appear to be attributable to activation differences during high wins, we examined among CPHIV effects of immune health in infancy on the high wins and win>loss contrasts only. Enrollment immune health data were available for 65 CPHIV which included all 57 CPHIV from the CHER cohort (enrollment age 6-12 weeks) and 8 from IMPAACT (enrollment age 22-88 weeks). 1 IMPAACT participant's data could not be found. 39 CPHIV had a high VL (>750,000 copies/mL) at enrollment and 26 had low VLs (400-750,000 copies/mL). Table 12 shows that the % BOLD signal change for high wins and win>loss in the cluster where CPHIV demonstrated smaller activation increases during processing of reward compared to loss were similar in CPHIV who had high and low viral loads (VL) in infancy. There was also no association of CD4 count at enrollment with % BOLD signal change during high wins (p=0.4874) or win>loss (p=0.157). However, increasing CD4% at enrollment was weakly associated, albeit below conventional levels of significance, with smaller % BOLD signal changes during high wins (Pearson r=-0.081; p=0.071) and for the win>loss contrast (r=-0.076; p=0.095) (Figure 9).

Table 12: Comparison in the ROI where CPHIV showed less activation during reward processing of the % BOLD signal change during high wins and win>loss between CPHIV who had high and low viral loads in infancy

	Mean % BOLD signal change ± Standard Deviation		1-tailed t-test
	CPHIV with High Viral Load (VL) in infancy (*N* = 39)	CPHIV with Low Viral Load (VL) in infancy (*N* = 26)	High VL vs Low VL
High Win	-0.11 ± 0.19	-0.13 ± 0.25	0.34
Win>Loss	-0.04 ± 0.18	-0.06 ± 0.20	0.38

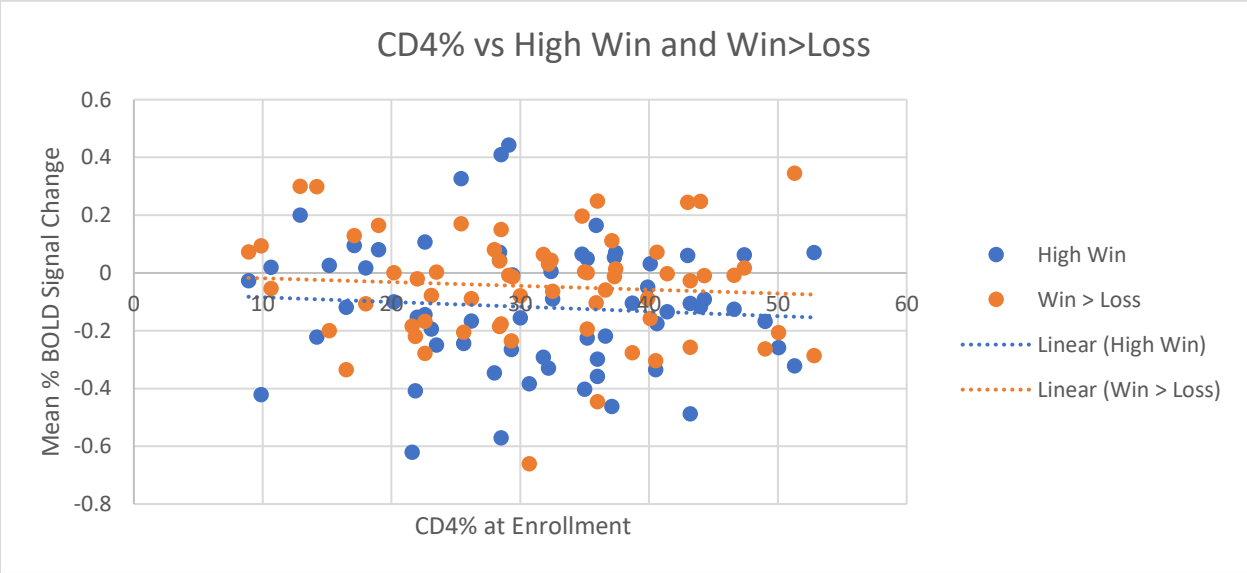

Figure 9: CD4% at enrollment vs mean % BOLD signal change for High Wins (blue) and Win>Loss (orange) in the left superior frontal cluster where CPHIV showed smaller activation increases than controls.

6. Discussion

With the initiation of early ART deemed safe (Cotton et al., 2013, Lowenthal et al., 2014) and its adoption globally for the treatment of infants and young children living with PHIV, hopes have grown for a new generation of CPHIV who would transition from childhood to adulthood as successfully as their uninfected peers. Adolescence is a critical cognitive developmental phase (Sowell et al., 2002) characterized by increasing independence and risk taking behaviours. Given the relationship between cognition and executive function, and the critical roles of working memory and reward processing in these (Luna, 2009), this project aimed to advance understanding of the effects of living with PHIV on reward processing networks. This may be a critical component of successful transitioning from childhood to adulthood.

In this study, we acquired functional MRI while 15-year-old adolescents with and without HIV performed the Reward Magnitude ("guessing") task to examine effects of living with HIV on brain function during reward processing.

Overall, CPHIV made their guesses during the fMRI task about 10% faster than their uninfected peers, suggesting less concern for or consideration of the consequences of their guesses. Adolescents in our cohort, irrespective of sex and HIV-status, demonstrated robust activation during reward processing (both win>loss and linear association with increasing positive reward) of the dorsal and ventral striatum and ventromedial prefrontal cortex – regions known to be involved in reward pathways. These regions were similarly activated in the study by Somerville et al. during performance of the Reward Magnitude Guessing Task (Somerville et al., 2018), confirming that our task setup is correct and that the task reliably activates reward circuits.

During anticipation ("stakes" vs rest) and processing of reward (win>loss and linear association with increasing positive reward) the whole sample (irrespective of HIV status) demonstrated greater activation bilaterally in the occipital cortices, middle frontal and precentral gyri, medially in the middle section of the cingulate gyrus, and either bilateral (anticipation) or right (reward) cerebellar cortices. During anticipation, we additionally observed increased activation of bilateral insula, a medial region in the superior frontal and paracingulate gyri, left inferior frontal gyrus, left temporal regions suggesting verbalizing of the stakes being played for, and the vermis. In contrast, reward processing additionally activated bilateral striatum, lateral frontal poles and

orbitofrontal cortices, a cluster in the medial paracingulate gyrus that extends into ventromedial prefrontal cortex, and right precuneus and fusiform cortices. Although both the contrasts win>loss (H2) and linear association with increasing positive reward (H4c) target reward processing, they produced a few activation clusters that differed – in the former (win>loss), greater activations were additionally seen in the right intracalcarine cortices, right middle and inferior temporal gyri, and in a left supramarginal gyrus / superior parietal lobule region, while greater activations with increasing positive reward were additionally observed in bilateral superior and middle frontal regions, and in the left insula.

Few regions demonstrated HIV-related differences in brain activation during either anticipation or reward processing. During anticipation, CPHIV demonstrated less activation than controls in 3 clusters located in the left occipital pole, left orbitofrontal cortex / temporal pole, and in the anterior cingulate / paracingulate gyrus (peak MNI coordinates: -0.5; 21; 37), respectively. For the win>loss contrast, CPHIV demonstrated smaller activation increases for wins compared to loss than controls in a region in the left superior and middle frontal gyrus (-20; 26; 39), which was shown to be largely attributable to the absence of activation increases in this region during high wins in the CPHIV. Surprisingly, despite the association of increasing age with larger signal increases in this region during processing of reward compared to punishment, *only* the signal change during high losses showed a weak trend-level inverse association with age. This finding suggests that the ability of older adolescents to more fully comprehend and process the implications of their actions and choices (i.e. improved decision-making skills), is likely attributable to better processing of negative feedback, rather than reward per sé. Two clusters in the same region {(-25; 28; 39) & (-29; 28; 49)} similarly showed smaller activation increases with increasing positive reward in CPHIV compared to controls (H4c), as well as a cluster in the left paracingulate gyrus (-8; 24; 51) that is superior to the region where CPHIV showed lower activation during anticipation. Males and females did not demonstrate any differences in the processing of either anticipation or reward.

6.1 Similarities in activation across contrasts

It is not surprising that some clusters showed activation on different contrasts. The task is visually appealing and also demands the participant to press a button – both these actions stimulate visual processing and motor neural activation/participation.

The largest activations across the different contrasts were in the bilateral occipital cortices. Since the occipital lobe is responsible for vision and visual processing, it plays a key role in working memory (Alan D. Baddeley, 1974), allowing the brain to use and interpret visual information. Visual processing is an important aspect of the Reward Magnitude task used in the present experiment, as participants need to interpret the "stakes" cue to appreciate the magnitude of the reward or loss they are playing for, and the "reward" feedback to comprehend whether they won or lost money. As such, it is not surprising that the occipital lobe was activated extensively across all the contrasts examined.

Second to the occipital lobe, the middle frontal and precentral gyri were activated during both anticipation and reward processing. The middle frontal cortex forms part of the prefrontal cortex which plays a key role in the management of higher cognitive functions such as decision-making (which includes planning, working memory, self-control, etc.). The primary motor cortex is located within the precentral gyri and is responsible for voluntary motor movements. The cerebellar cortices that were also activated play a role in both cognitive functions (lobules VI, VIIb, Crus I, and Crus II) and fine motor processes (vermis). During the task the participants were required to make a guess (decision) and record that decision by pressing a button with their index or middle fingers.

Finally, the cingulate gyrus, which was also activated during anticipation and reward processing, forms a major part of the limbic system. The limbic system is involved in processing and regulating emotion and memory, and is vital to cognitive functions, such as reward and loss anticipation, decision-making and working memory. Therefore, the activation of the cingulate gyrus was to be expected given the anticipation, guessing/decision-making, and reward processing nature of the task.

6.2 Contrast: H1

In contrast H1 we considered "stakes" vs rest. During the "stakes" cue, participants view either the High Stakes or the Low Stakes screens, which introduces the subsequent set of trials and creates a sense of anticipation regarding the "importance" of the guesses that will follow.

During anticipation, we additionally observed increased activation of bilateral insula. It has been suggested that the insular cortices and cingulate gyrus are involved in the emotional aspects of risky decision-making (Uddin et al., 2017), as well as anticipation (Jauhar et al., 2021). Van Leijenhorst et al. examined neural differences in three adolescent age groups, i.e., 10-12 years, 14-15 years, and 18-23 years old. Their study sample was comprised of 53 healthy participants from the Netherlands. The study design was similar to that of our study, with participants undergoing fMRI scanning while performing an interactive reward incentive task. During anticipation they found bilateral anterior insular activation in their 10-12 and 14-15 year-old age groups (Van Leijenhorst et al., 2010b). Jauhar et al. (2021) in their study investigating brain activations associated with anticipation and delivery of monetary reward, found that only reward anticipation was associated with activations outside the medial cortical surface, which were located in the bilateral insula bilaterally (Jauhar et al., 2021).

Furthermore, we found increased activation during anticipation in the left inferior frontal gyrus responsible for cognitive function, as well as in the left temporal regions involved in understanding language and learning and remembering verbal information, suggesting verbalizing of the stakes being played for, and the vermis, which Kruithof et al. also reliably found to be activated during anticipation (Kruithof et al., 2023).

6.3 Contrast: H2 and H4c

Contrasts H2 and H4c identified brain regions activated more during processing of reward than loss/punishment. As mentioned, adolescents are more prone to taking risks. It is known that, during adolescence, neural systems driven by dopamine (which include cognitive and limbic regions) undergo rigorous development due to synaptic pruning and ongoing myelination (Sowell et al., 2002, Telzer, 2016, Ismail et al., 2017, Paus, 2010, Paus et al., 2001, Power et al., 2010, Fair et al., 2009). Studies involving monetary rewards have found that, during adolescence, activation in the ventral striatum are significantly greater than during childhood and adulthood (Ernst et al.,

2005, Van Leijenhorst et al., 2010a), and that this increase is coupled with a decrease in cognitive control (Somerville et al., 2011, Van Leijenhorst et al., 2010a). This imbalance in reward and regulatory brain circuitry during adolescence is attributed to varying rates of development of limbic and prefrontal brain regions (Van Leijenhorst et al., 2010b). Brain maturation occurs in a posterior–anterior direction, with higher-order cognitive functions utilizing prefrontal and parietal cortical regions maturing only in late childhood and adolescence (Toga et al., 2006, Khundrakpam et al., 2013, Khundrakpam et al., 2016). Imbalance between the largely mature limbic reward circuitry and the immature prefrontal executive function regions may account for the observed increases in risk-taking behaviours during adolescence (Giedd, 2010, Paus et al., 2008).

Since the reward processing networks, which include both the ventral and dorsal striatum and other associated regions, continue to develop throughout adolescence, these regions can be considered a plastic system (Ismail et al., 2017). Its development is therefore vulnerable and can be shaped by negative or positive experiences (Reynolds and Flores, 2021) and/or insults to the brain.

Overall, the brain regions where we found greater activation specifically during processing of reward than loss, namely the bilateral striatum, lateral frontal poles and orbitofrontal cortices, medial paracingulate gyrus extending into ventromedial prefrontal cortex, and right precuneus and fusiform cortices, agree with findings from others. However, some studies have reported activation of similar networks during processing of reward and loss, while others have reported distinct networks.

For example, Camara et al. (2008) conducted a study where they also used a monetary task-based fMRI approach to investigate brain activation, as well as functional connectivity to a ventral striatal seed region, during processing of reward and loss. For both reward and loss, they found similar activations in a fronto-subcortical-parietal network, including both the dorsal and ventral striatum, the anterior cingulate cortex (ACC) in the ventromedial prefrontal cortex, lateral frontal poles and orbitofrontal cortices. For the contrast gain versus loss, greater activations were observed bilaterally in the ventral striatum. Moreover, signals in the insular cortex, the amygdala and the hippocampus were similar for reward and loss and were correlated to activity in the

ventral striatum. However, functional connectivity of the ventral striatum to the amygdala and medial orbitofrontal cortices were larger after losses. Notably, the ventral striatum and prefrontal cortices form part of the mesocorticolimbic (MCL) system (red and yellow reward pathways in figure 1) (Camara et al., 2008).

In contrast to the study by Camara et al. (2008), Oldham et al. (2018) in a study examining brain activation during anticipation and the outcome phases of reward and loss processing using neuroimaging and a task design much like ours, only found activation of the orbitofrontal and ventromedial prefrontal regions during reward outcomes (Oldham et al., 2018).

In a study examining risky sexual behaviours in adolescents and its association with activity in social reward networks, adolescents with higher-risk sexual behaviours showed greater activation increases during social reward feedback blocks compared to neutral blocks in the right precuneus and right temporoparietal junction (Eckstrand et al., 2017). Social reward blocks consisted of photos of peers who had ostensibly rated a picture of the individual favourably, i.e. that they felt they would like the participant, as opposed to neutral blocks, which consisted of photos of peers that had provided no feedback or rating of the individual's photo. The temporoparietal junction – a component of the default mode network – is involved in processing socially-relevant information, while the precuneus has been implicated in autobiographical memory, self, and agency (Krall et al., 2015). The authors postulate that the greater activation in self-referential and social reward processing regions among adolescents with higher-risk sexual behaviours suggest a greater sensitivity to social rewards among these youth. In our study, greater activation during processing of wins than losses of the precuneus and the fusiform cortices, which also play a role in image memory retrieval, may therefore point to greater self-referential behaviour during receipt of reward, i.e., a greater tendency to relate positive than negative feedback to the self.

Although both the contrasts win>loss (H2) and linear association with increasing positive reward (H4c) target reward processing, they produced a few activation clusters that differed. In the win>loss contrast, greater activations were additionally seen in the left supramarginal gyrus / superior parietal lobule region, while increasing positive reward was associated with greater activations in bilateral superior and middle frontal regions, and in the left insula. This finding is

consistent with that of Polack et al. (2023) who demonstrated using the monetary incentive delay (MID) task (Knutson et al., 2000) that some regions involved in reward processing from pre- to early adolescence are sensitive to either reward valence (i.e., win vs loss) or magnitude (Gadassi Polack et al., 2023). In the MID task, there are 5 trial types: high or low wins or losses, or no money at stake. After a cue displaying the trial type, a target is displayed for 150-500 ms. A button press by the participant during the display of the target is considered a successful response (success feedback) and may result in monetary win, while failing to press the button while the target is displayed is considered a failure (failure feedback) and may result in monetary loss. As such, success feedback includes wins and no wins, while failure feedback includes no wins and losses. This task therefore allows valence and magnitude to be examined for each of the 3 conditions – anticipation, success feedback and failure feedback. Since in our study contrast H2 (win vs loss) does not consider reward magnitude, but winning as a whole vs losing as a whole, whereas contrasts H4a-H4c consider the effects of reward magnitude specifically, regions activated by one but not the other reflect sensitivity to either valence (H2) or magnitude (H4). The regions where we found sensitivity to either valence or magnitude are consistent with those reported by Polack et al. (2023). Specifically, Polack et al. also found that the left supramarginal gyrus was sensitive to valence during success feedback, while the bilateral superior frontal gyri and left insula were sensitive to magnitude both during anticipation and success feedback. Notably, they found that during anticipation and success feedback, the left supramarginal and right superior frontal gyri, respectively, were sensitive *only* to money being at stake.

6.4 Contrast: H4a and H4b

As mentioned in the paragraph above, there are multiple regions in the reward processing network of the brain that are sensitive to either valence or reward magnitude. Contrast H4a considers the effect of the magnitude of the reward received (winning) on brain activation, whereas contrast H4b considers the effect of the magnitude of the punishment (losing, or what Leijenhorst et al. refer to as the omission of reward (Van Leijenhorst et al., 2010b)). The ability of the brain to distinguish between large and small monetary gains/losses allows individuals to make value-based decisions which correlates to different behavioural outcomes.

When comparing high and low wins in the whole sample, we found greater activation for high wins bilaterally in the occipital, fusiform, insular and intracalcarine cortices, and pre- and postcentral gyri, the right inferior, middle and superior temporal gyri, right middle frontal / precentral gyrus, left cerebellar cortex, and a medial posterior cingulate / precuneus region. Polack et al. (2023) also found sensitivity to magnitude during success feedback conditions in occipital, insular and fusiform regions.

We did not find any significant differences in neural activity when comparing low and high loss outcomes. The absence of activation differences between low and high losses suggests that at this age adolescents may be more win-orientated. This is consistent with our findings suggesting greater self-referential behaviour during receipt of reward. Notably, Polack et al. also identified fewer regions with sensitivity to magnitude during their failure feedback conditions than during the success feedbacks.

6.5 CPHIV vs Controls

During anticipation, CPHIV demonstrated less activation than controls in 3 clusters located in the left occipital pole, left orbitofrontal cortex / temporal pole, and in the anterior cingulate / paracingulate gyrus, respectively. All three of these clusters are involved in executive functions and cognitive processes, including visuospatial processing, object recognition, memory formation, controlling and correcting reward-related and punishment-related behaviour, decision-making and working memory (Rehman and Khalili, 2023, Rolls, 2004, Apps et al., 2016). Notably, the anterior cingulate is located in the ventromedial prefrontal cortex – a key component of the reward processing circuit.

While we found no differences between CPHIV and controls during reward processing in the parts of the reward circuit where activation was seen in all adolescents, CPHIV demonstrated less activation than controls during reward processing (H2) in a small left superior and middle frontal cluster, which was shown to be largely attributable to the absence of activation increases in this region during high wins in the CPHIV. This finding suggests that brain regions involved in the reward circuit in controls may be more extensive than in CPHIV. Notably, the region showing less activity in CPHIV is involved in the working memory component of executive function.

Similar to the difference seen between CPHIV and controls during reward processing (win>loss), CPHIV showed smaller activation increases with increasing reward in two left superior and middle frontal clusters – one of which overlaps exactly with the cluster where smaller activation increases were seen for wins compared to losses, as well as a cluster in the left paracingulate gyrus (-8; 24; 51) that is superior to the region where CPHIV showed lower activation during anticipation. All these regions are involved in executive functions and can be seen in figure 10.

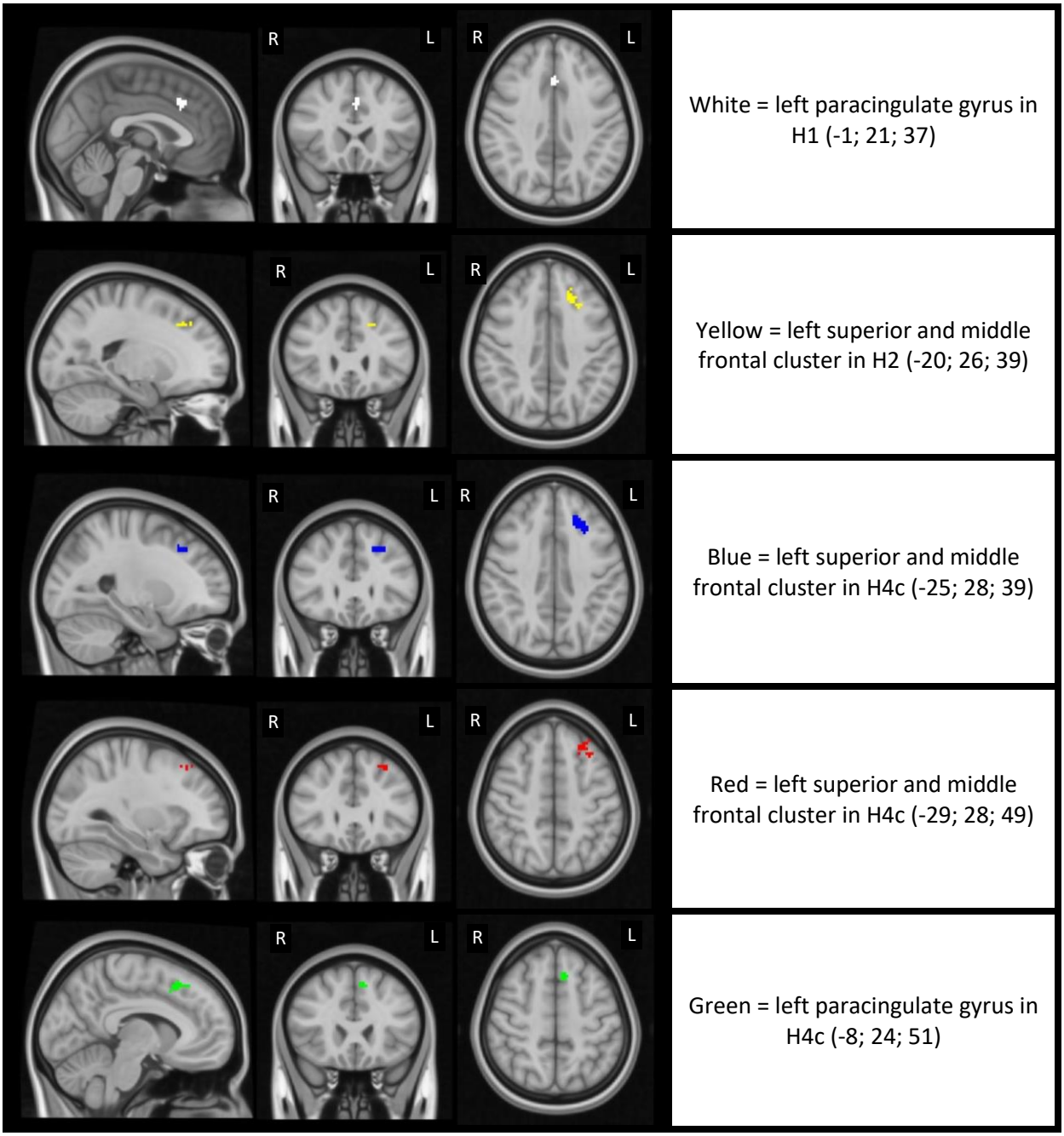

Figure 10: Clusters where CPHIV showed less activation than controls on the various contrasts. R = Right; L = Left; Z>3.1 and a cluster significance threshold of p=0.05. H1 anticipation; H2 win>loss; H4c increasing activation with increasing reward.

Working memory refers to the storage and manipulation of small amounts of information in the brain to ensure successful execution of tasks (Cowan, 2014). Notably, instantaneous/short-term information received and manipulated by working memory, much like the “stakes” slide in our

task, are not necessarily only stored by the brain for a small amount of time, but can contribute to long-term memory (Chai et al., 2018).

Baddeley and Hitch's working memory model (Alan D. Baddeley, 1974) proposes four subcomponents of working memory, i.e., the phonological (auditory) loop, the visuospatial loop, the episodic buffer, and the central executive. The phonological loop deals with information that is obtained during written and spoken language. The visuospatial loop handles visual information and spatial co-ordination, making people aware of their location in relation to visual objects. The episodic buffer plays an important role in how and when short-term memories become long-term. The central executive importantly deals with switching between loops to stimulate different memories, as a combination of memories are often needed to complete a task.

With our task being visually enticing, the visuospatial loop within working memory may be particularly important. Poor visuospatial working memory performance relative to age-appropriate norms has been reported previously in 6- to 14-year-old CPHIV (Koekkoek et al., 2008). A Ugandan study found executive function deficits in CPHIV aged 6-12 years, particularly on visual planning and reasoning (Ruel et al., 2012), and Hoare et al. (2012) reported deficits in similarly aged CPHIV in visual memory, visuospatial processing, and executive functioning (Hoare et al., 2012). In view of the visual nature of the present task, including the need to remember the 'stakes' being played for and to process the reward/loss feedback, deficits in visuospatial working memory may play a role in altered reward processing. Reduced activation increases in CPHIV in superior and middle frontal working memory regions during trials with positive compared to negative feedback (win>loss), suggest that CPHIV do not benefit to the same extent from a positive outcome or reward. Further investigation of brain activity within the region where we found differences on reward processing between CPHIV and controls, revealed that the smaller activation increases seen for wins compared to losses in CPHIV are attributable to reduced activation during high wins (Fig. 4). Essentially, CPHIV fail to demonstrate the increases in brain activity that are seen in controls in the implicated superior and middle frontal cluster following high win feedbacks. Specifically, reduced processing or 'remembering' of high wins in CPHIV may lead to increased risk-taking behaviour to achieve similar reward experiences as controls.

Van Leijenhorst et al. found that the middle-aged adolescent group (aged 14-15 years) were more responsive to reward receipt than the omission thereof compared to the rest of the cohort based on greater activation in the ventral striatum (Van Leijenhorst et al., 2010b). Given that the ventral striatum and our small cluster in the left superior and middle frontal gyrus (ROI) both form part of the mesocorticolimbic system, and that the middle-aged adolescent group demonstrated greater activation of this system than 10-12 year old children, the reduced activations seen within this system in our study may point to developmental delay in CPHIV. Interestingly, activation increases for wins compared to losses in this region did increase with age, however, posthoc analyses revealed that this was largely attributable to larger deactivations with increasing age during high losses – perhaps reflecting a greater ability of older adolescents to more fully process the implications of a loss. CPHIV also responded faster on all trials (high- and low-stakes trials) than controls, suggesting that they were perhaps less concerned with the outcome of their choice.

6.6 Limitations

In our study we aimed to investigate among adolescents the effects of living with HIV on neural circuits involved in reward processing, to ascertain whether children with PHIV are at greater risk for risk-taking behaviours. In our cohort, specifically, there are many aspects, such as poor socioeconomic status that could influence our findings. Participants were recruited from historically disadvantaged communities characterised by poor education and high levels of substance and alcohol use. However, to minimise potential confounding by these factors, CPHIV and controls were recruited from the same communities. At the time of the study, we know that our participants were relatively healthy. We did not, however, control for previous diagnoses of HIV encephalopathy or other serious illnesses that may have caused neural damage. Notably, among CPHIV, brain activations in the region showing HIV-related damage did not show any association (at conventional levels of significance, $p<0.05$) with any markers of infant immune health, suggesting that alterations seen here are due to ongoing HIV effects rather than early damage.

Furthermore, there are also various limitations to using fMRI as our means of imagery, as well as statistical concerns (i.e. power). Specifically, fMRI has low spatial resolution, suffers from partial

volume effects, is an indirect measure of brain activation, produces a signal change that is typically one percent or less making it difficult to separate from noise, and may be confounded by motion.

Since the aim of this study was to identify HIV-related changes in reward processing, and these may not be limited to known reward processing networks, we chose to perform whole-brain voxelwise analyses. However, this involves repeating statistical analyses for >100,000 voxels in the brain, requiring multiple comparison correction. Here we used cluster-size based thresholding to correct for multiple comparisons, due to its higher sensitivity compared to other methods to weak and diffuse signals. However, this approach provides low spatial specificity as the precise location of the activation within a cluster cannot be determined. Given that reward processing tends to engage a well-delineated set of brain regions including the ventral striatum, a priori hypothesis-driven region-of-interest analyses targeting those regions is an alternative strategy that should be explored in future work.

6.7 Future Work

Since adolescence is a time during which the brain still undergoes development not only because of pubertal influences, but also external societal influences (Giedd, 2010), it would be of great importance to investigate this cohort after adolescence, when the neural developmental trajectory has decreased and puberty has been reached fully. The functional neural differences seen between CPHIV and controls during adolescence may resolve as the cohort grows older, pointing to HIV-related developmental delay, or may persist, pointing to permanent neural damage.

Furthermore, examining associations of brain activations during reward processing with behavioural/cognitive assessments of working memory and risk-taking behaviour would elucidate the relation between these two functional domains, whether they form part of a greater network, as well as advance understanding of the HIV-related differences seen here and their implications.

In the present study, effects of HIV on reward processing was limited to small, localised left superior frontal clusters. However, given that all CPHIV in the present study had initiated ART before age 18 months, these findings may not translate to CPHIV who had started ART later in

life. A longer period of unsuppressed HIV may well result in greater functional deficits. As such, future studies should examine how the severity and duration of unsuppressed HIV infection affects neural circuits involved in reward processing, and whether there is a particular age that unsuppressed HIV is most detrimental to development and cognitive functioning.

7. Conclusion

In this study, we investigated in adolescents the effects of living with HIV on neural circuits involved in reward processing. Using FMRI and the Reward Magnitude Task we found reliable activation of striatal and medial frontal regions involved in decision-making and in reward processing. No differences were found in these particular reward processing networks when comparing CPHIV and controls, nor when comparing males and females, for any of the contrasts examined. Overall, these findings point to largely intact reward processing networks in CPHIV. However, there were small distributed clusters in the left hemisphere where CPHIV demonstrated smaller activation increases during wins than controls – 2 distinct clusters in the left superior and middle frontal gyri, and one in the left paracingulate gyrus – and during anticipation – 3 clusters in the left occipital pole, left temporal pole / orbitofrontal cortex, and left paracingulate gyrus. Notably, except for the occipital pole, all these regions are involved in working memory and are directly adjacent to the medial frontal regions of the reward circuit. Furthermore, this difference was shown to be attributable to smaller activation increases during high reward trials in CPHIV. These findings suggest that HIV-related working memory impairment may impact reward processing. Specifically, reduced processing or 'remembering' of high wins in CPHIV may lead to increased risk-taking behaviour to achieve similar reward experiences as controls.

References

ACKERMANN, C., ANDRONIKOU, S., LAUGHTON, B., KIDD, M., DOBBELS, E., INNES, S., VAN TOORN, R. & COTTON, M. 2014. White matter signal abnormalities in children with suspected HIV-related neurologic disease on early combination antiretroviral therapy. *Pediatr Infect Dis J,* 33**,** e207-12.

ACKERMANN, C., ANDRONIKOU, S., SALEH, M. G., LAUGHTON, B., ALHAMUD, A. A., VAN DER KOUWE, A., KIDD, M., COTTON, M. F. & MEINTJES, E. M. 2016. Early Antiretroviral Therapy in HIV-Infected Children Is Associated with Diffuse White Matter Structural Abnormality and Corpus Callosum Sparing. *AJNR Am J Neuroradiol,* 37**,** 2363-2369.

ALAN D. BADDELEY, G. H. 1974. Working Memory. *Psychology of Learning and Motivation,* 8**,** 47-89.

APPS, M. A., RUSHWORTH, M. F. & CHANG, S. W. 2016. The Anterior Cingulate Gyrus and Social Cognition: Tracking the Motivation of Others. *Neuron,* 90**,** 692-707.

BAARS, N. G. B. 2018. *Fundamentals of Cognitive Neuroscience: A Beginner's Guide*, Academic Press.

BARLOW-MOSHA, L., ANGELIDOU, K., LINDSEY, J., ARCHARY, M., COTTON, M., DITTMER, S., FAIRLIE, L., KABUGHO, E., KAMTHUNZI, P., KINIKAR, A., MBENGERANWA, T., MSUYA, L., SAMBO, P., PATEL, K., BARR, E., JEAN-PHILLIPE, P., VIOLARI, A., MOFENSON, L., PALUMBO, P. & CHI, B. H. 2016. Nevirapine- Versus Lopinavir/Ritonavir-Based Antiretroviral Therapy in HIV-Infected Infants and Young Children: Long-term Follow-up of the IMPAACT P1060 Randomized Trial. *Clin Infect Dis,* 63**,** 1113-1121.

BLAKEMORE, S. J. & CHOUDHURY, S. 2006. Development of the adolescent brain: implications for executive function and social cognition. *J Child Psychol Psychiatry,* 47**,** 296-312.

BOIVIN, M. J., BARLOW-MOSHA, L., CHERNOFF, M. C., LAUGHTON, B., ZIMMER, B., JOYCE, C., BWAKURA-DANGAREMBIZI, M., RATSWANA, M., ABRAHAMS, N., FAIRLIE, L., GOUS, H., KAMTHUNZI, P., MCCARTHY, K., FAMILIAR-LOPEZ, I., JEAN-PHILLIPPE, P., COETZEE, J., VIOLARI, A., COTTON, M. F., PALUMBO, P. E. & TEAM, I. P. S. 2018. Neuropsychological performance in African children with HIV enrolled in a multisite antiretroviral clinical trial. *AIDS,* 32**,** 189-204.

BUXTON, R. B. 2002. *Introduction to Functional Magnetic Resonance Imaging: Priciples & Techniques,* United States of America, New York, Cambridge University Press.

CAMARA, E., RODRIGUEZ-FORNELLS, A. & MUNTE, T. F. 2008. Functional connectivity of reward processing in the brain. *Front Hum Neurosci,* 2**,** 19.

CHAI, W. J., ABD HAMID, A. I. & ABDULLAH, J. M. 2018. Working Memory From the Psychological and Neurosciences Perspectives: A Review. *Front Psychol,* 9**,** 401.

CLUVER, L. D., ORKIN, M., GARDNER, F. & BOYES, M. E. 2012. Persisting mental health problems among AIDS-orphaned children in South Africa. *J Child Psychol Psychiatry,* 53**,** 363-70.

COTTON, M. F., VIOLARI, A., OTWOMBE, K., PANCHIA, R., DOBBELS, E., RABIE, H., JOSIPOVIC, D., LIBERTY, A., LAZARUS, E., INNES, S., VAN RENSBURG, A. J., PELSER, W., TRUTER, H., MADHI, S. A., HANDELSMAN, E., JEAN-PHILIPPE, P., MCINTYRE, J. A., GIBB, D. M., BABIKER, A. G. & TEAM, C. S. 2013. Early time-limited antiretroviral therapy versus deferred therapy in South African infants infected with HIV: results from the children with HIV early antiretroviral (CHER) randomised trial. *Lancet,* 382**,** 1555-63.

COWAN, N. 2014. Working Memory Underpins Cognitive Development, Learning, and Education. *Educ Psychol Rev,* 26**,** 197-223.

PLESSIS, S. D., VINK, M., JOSKA, J. A., KOUTSILIERI, E., STEIN, D. J. & EMSLEY, R. 2014. HIV infection and the fronto-striatal system: a systematic review and meta-analysis of fMRI studies. *AIDS,* 28**,** 803-11.

PLESSIS, S., VINK, M., JOSKA, J. A., KOUTSILIERI, E., BAGADIA, A., STEIN, D. J. & EMSLEY, R. 2015. HIV infection results in ventral-striatal reward system hypo-activation during cue processing. *AIDS,* 29**,** 1335-43.

ECKSTRAND, K. L., CHOUKAS-BRADLEY, S., MOHANTY, A., CROSS, M., ALLEN, N. B., SILK, J. S., JONES, N. P. & FORBES, E. E. 2017. Heightened activity in social reward networks is associated with adolescents' risky sexual behaviors. *Dev Cogn Neurosci,* 27**,** 1-9.

ERNST, M., NELSON, E. E., JAZBEC, S., MCCLURE, E. B., MONK, C. S., LEIBENLUFT, E., BLAIR, J. & PINE, D. S. 2005. Amygdala and nucleus accumbens in responses to receipt and omission of gains in adults and adolescents. *Neuroimage,* 25**,** 1279-91.

ESTEBAN, O., MARKIEWICZ, C. J., BLAIR, R. W., MOODIE, C. A., ISIK, A. I., ERRAMUZPE, A., KENT, J. D., GONCALVES, M., DUPRE, E., SNYDER, M., OYA, H., GHOSH, S. S., WRIGHT, J., DURNEZ, J., POLDRACK, R. A. & GORGOLEWSKI, K. J. 2019. fMRIPrep: a robust preprocessing pipeline for functional MRI. *Nat Methods,* 16**,** 111-116.

EZEAMAMA, A. E., KIZZA, F. N., ZALWANGO, S. K., NKWATA, A. K., ZHANG, M., RIVERA, M. L., SEKANDI, J. N., KAKAIRE, R., KIWANUKA, N. & WHALEN, C. C. 2016. Perinatal HIV Status and Executive Function During School-Age and Adolescence: A Comparative Study of Long-Term Cognitive Capacity Among Children From a High HIV Prevalence Setting. *Medicine (Baltimore),* 95**,** e3438.

FAIR, D. A., COHEN, A. L., POWER, J. D., DOSENBACH, N. U., CHURCH, J. A., MIEZIN, F. M., SCHLAGGAR, B. L. & PETERSEN, S. E. 2009. Functional brain networks develop from a "local to distributed" organization. *PLoS Comput Biol,* 5**,** e1000381.

FEINBERG, D. A., MOELLER, S., SMITH, S. M., AUERBACH, E., RAMANNA, S., GUNTHER, M., GLASSER, M. F., MILLER, K. L., UGURBIL, K. & YACOUB, E. 2010. Multiplexed echo planar imaging for sub-second whole brain FMRI and fast diffusion imaging. *PLoS One,* 5**,** e15710.

GADASSI POLACK, R., MOLLICK, J. A., KEREN, H., JOORMANN, J. & WATTS, R. 2023. Neural responses to reward valence and magnitude from pre- to early adolescence. *Neuroimage,* 275**,** 120166.

GALVAN, A. 2010. Adolescent development of the reward system. *Front Hum Neurosci,* 4**,** 6.

GALVAN, A., VAN LEIJENHORST, L. & MCGLENNEN, K. M. 2012. Considerations for imaging the adolescent brain. *Dev Cogn Neurosci,* 2**,** 293-302.

GIEDD, J. N. 2010. The Teen Brain: Primed to Learn, Primed to Take Risks. *Cerebrum*.

GODDINGS, A. L., MILLS, K. L., CLASEN, L. S., GIEDD, J. N., VINER, R. M. & BLAKEMORE, S. J. 2014. The influence of puberty on subcortical brain development. *Neuroimage,* 88**,** 242-51.

GOVERNMENT, W. C. 2022. *Grades R-9* [Online]. Available: https://www.westerncape.gov.za/service/grades-r-9 [Accessed].

HARTLEY, C. A. & SOMERVILLE, L. H. 2015. The neuroscience of adolescent decision-making. *Curr Opin Behav Sci,* 5**,** 108-115.

HERTING, M. M., UBAN, K. A., WILLIAMS, P. L., GAUTAM, P., HUO, Y., MALEE, K., YOGEV, R., CSERNANSKY, J., WANG, L., NICHOLS, S., VAN DYKE, R. & SOWELL, E. R. 2015. Default Mode Connectivity in Youth With Perinatally Acquired HIV. *Medicine (Baltimore),* 94**,** e1417.

HIV.GOV. 2020. *What are HIV and AIDS?* [Online]. HIV.gov. Available: https://www.hiv.gov/hiv-basics/overview/about-hiv-and-aids/what-are-hiv-and-aids [Accessed].

HOARE, J., FOUCHE, J. P., PHILLIPS, N., JOSKA, J. A., MYER, L., ZAR, H. J. & STEIN, D. J. 2018. Structural brain changes in perinatally HIV-infected young adolescents in South Africa. *AIDS,* 32**,** 2707-2718.

HOARE, J., FOUCHE, J. P., SPOTTISWOODE, B., DONALD, K., PHILIPPS, N., BEZUIDENHOUT, H., MULLIGAN, C., WEBSTER, V., ODURO, C., SCHRIEFF, L., PAUL, R., ZAR, H., THOMAS, K. & STEIN, D. 2012. A diffusion tensor imaging and neurocognitive study of HIV-positive children who are HAART-naive "slow progressors". *J Neurovirol,* 18**,** 205-12.

ISMAIL, F. Y., FATEMI, A. & JOHNSTON, M. V. 2017. Cerebral plasticity: Windows of opportunity in the developing brain. *Eur J Paediatr Neurol,* 21**,** 23-48.

JANKIEWICZ, M., HOLMES, M. J., TAYLOR, P. A., COTTON, M. F., LAUGHTON, B., VAN DER KOUWE, A. J. W. & MEINTJES, E. M. 2017. White Matter Abnormalities in Children with HIV Infection and Exposure. *Front Neuroanat,* 11**,** 88.

JAUHAR, S., FORTEA, L., SOLANES, A., ALBAJES-EIZAGIRRE, A., MCKENNA, P. J. & RADUA, J. 2021. Brain activations associated with anticipation and delivery of monetary reward: A systematic review and meta-analysis of fMRI studies. *PLoS One,* 16**,** e0255292.

KATHARINE HALL, A. D. L. 2019. Children's access to education. ChildGauge.

KHUNDRAKPAM, B. S., LEWIS, J. D., ZHAO, L., CHOUINARD-DECORTE, F. & EVANS, A. C. 2016. Brain connectivity in normally developing children and adolescents. *Neuroimage,* 134**,** 192-203.

KHUNDRAKPAM, B. S., REID, A., BRAUER, J., CARBONELL, F., LEWIS, J., AMEIS, S., KARAMA, S., LEE, J., CHEN, Z., DAS, S., EVANS, A. C. & BRAIN DEVELOPMENT COOPERATIVE, G. 2013. Developmental changes in organization of structural brain networks. *Cereb Cortex,* 23**,** 2072-85.

KNUTSON, B., WESTDORP, A., KAISER, E. & HOMMER, D. 2000. FMRI visualization of brain activity during a monetary incentive delay task. Neuroimage, 12, 20-7.

KOEKKOEK, S., DE SONNEVILLE, L. M., WOLFS, T. F., LICHT, R. & GEELEN, S. P. 2008. Neurocognitive function profile in HIV-infected school-age children. *Eur J Paediatr Neurol,* 12**,** 290-7.

KRALL, S. C., ROTTSCHY, C., OBERWELLAND, E., BZDOK, D., FOX, P. T., EICKHOFF, S. B., FINK, G. R. & KONRAD, K. 2015. The role of the right temporoparietal junction in attention and social interaction as revealed by ALE meta-analysis. Brain Struct Funct, 220, 587-604.

KRUITHOF, E. S., KLAUS, J. & SCHUTTER, D. 2023. The human cerebellum in reward anticipation and outcome processing: An activation likelihood estimation meta-analysis. Neurosci Biobehav Rev, 149, 105171.

LAUGHTON, B., CORNELL, M., BOIVIN, M. & VAN RIE, A. 2013. Neurodevelopment in perinatally HIV-infected children: a concern for adolescence. *J Int AIDS Soc,* 16**,** 18603.

LAUGHTON, B., CORNELL, M., KIDD, M., SPRINGER, P. E., DOBBELS, E. F. M., RENSBURG, A. J. V., OTWOMBE, K., BABIKER, A., GIBB, D. M., VIOLARI, A., KRUGER, M. & COTTON, M. F. 2018. Five year neurodevelopment outcomes of perinatally HIV-infected children on early limited or deferred continuous antiretroviral therapy. *J Int AIDS Soc,* 21**,** e25106.

LE DOARE, K., BLAND, R. & NEWELL, M. L. 2012. Neurodevelopment in children born to HIV-infected mothers by infection and treatment status. *Pediatrics,* 130**,** e1326-44.

LESAGE, E., STEIN, E.A 2016. Networks Associated with Reward. *Neuroscience in the 21st Century*.

LEWIS-DE LOS ANGELES, C. P., WILLIAMS, P. L., JENKINS, L. M., HUO, Y., MALEE, K., ALPERT, K. I., UBAN, K. A., HERTING, M. M., CSERNANSKY, J. G., NICHOLS, S. L., VAN DYKE, R. B., SOWELL, E. R., WANG, L., PEDIATRIC, H. I. V. A. C. S., THE PEDIATRIC IMAGING, N. & GENETICS, S. 2020. Brain morphometric differences in youth with and without perinatally-acquired HIV: A cross-sectional study. *Neuroimage Clin,* 26**,** 102246.

LIU, Y., ZHANG, Y., JIANG, Z., KONG, W. & ZOU, L. 2023. Exploring Neural Mechanisms of Reward Processing Using Coupled Matrix Tensor Factorization: A Simultaneous EEG-fMRI Investigation. *Brain Sci,* 13.

LORIN, V., DANCKAERT, A., PORROT, F., SCHWARTZ, O., AFONSO, P. V. & MOUQUET, H. 2020. Antibody Neutralization of HIV-1 Crossing the Blood-Brain Barrier. *mBio,* 11.

LOWENTHAL, E. D., BAKEERA-KITAKA, S., MARUKUTIRA, T., CHAPMAN, J., GOLDRATH, K. & FERRAND, R. A. 2014. Perinatally acquired HIV infection in adolescents from sub-Saharan Africa: a review of emerging challenges. *Lancet Infect Dis,* 14**,** 627-39.

LUNA, B. 2009. Developmental changes in cognitive control through adolescence. *Adv Child Dev Behav,* 37**,** 233-78.

MBUGUA, K. K., HOLMES, M. J., COTTON, M. F., RATAI, E. M., LITTLE, F., HESS, A. T., DOBBELS, E., VAN DER KOUWE, A. J., LAUGHTON, B. & MEINTJES, E. M. 2016. HIV-associated CD4+/CD8+ depletion in infancy is associated with neurometabolic reductions in the basal ganglia at age 5 years despite early antiretroviral therapy. *AIDS,* 30**,** 1353-62.

MOELLER, S., YACOUB, E., OLMAN, C. A., AUERBACH, E., STRUPP, J., HAREL, N. & UGURBIL, K. 2010. Multiband multislice GE-EPI at 7 tesla, with 16-fold acceleration using partial parallel imaging with application to high spatial and temporal whole-brain fMRI. *Magn Reson Med,* 63**,** 1144-53.

NWOSU, E. C., ROBERTSON, F. C., HOLMES, M. J., COTTON, M. F., DOBBELS, E., LITTLE, F., LAUGHTON, B., VAN DER KOUWE, A. & MEINTJES, E. M. 2018. Altered brain morphometry in 7-year old HIV-infected children on early ART. *Metab Brain Dis,* 33**,** 523-535.

OLDHAM, S., MURAWSKI, C., FORNITO, A., YOUSSEF, G., YUCEL, M. & LORENZETTI, V. 2018. The anticipation and outcome phases of reward and loss processing: A neuroimaging meta-analysis of the monetary incentive delay task. *Hum Brain Mapp,* 39**,** 3398-3418.

OSBORNE, O., PEYRAVIAN, N., NAIR, M., DAUNERT, S. & TOBOREK, M. 2020. The Paradox of HIV Blood-Brain Barrier Penetrance and Antiretroviral Drug Delivery Deficiencies. *Trends Neurosci,* 43**,** 695-708.

PAUS, T. 2010. Growth of white matter in the adolescent brain: myelin or axon? *Brain Cogn,* 72**,** 26-35.

PAUS, T., COLLINS, D. L., EVANS, A. C., LEONARD, G., PIKE, B. & ZIJDENBOS, A. 2001. Maturation of white matter in the human brain: a review of magnetic resonance studies. *Brain Res Bull,* 54**,** 255-66.

PAUS, T., KESHAVAN, M. & GIEDD, J. N. 2008. Why do many psychiatric disorders emerge during adolescence? *Nat Rev Neurosci,* 9**,** 947-57.

POWER, J. D., FAIR, D. A., SCHLAGGAR, B. L. & PETERSEN, S. E. 2010. The development of human functional brain networks. *Neuron,* 67**,** 735-48.

PUTHANAKIT, T., AURPIBUL, L., LOUTHRENOO, O., TAPANYA, P., NADSASARN, R., INSEE-ARD, S. & SIRISANTHANA, V. 2010. Poor cognitive functioning of school-aged children in thailand with perinatally acquired HIV infection taking antiretroviral therapy. *AIDS Patient Care STDS,* 24**,** 141-6.

PUTHANAKIT, T., SAPHONN, V., ANANWORANICH, J., KOSALARAKSA, P., HANSUDEWECHAKUL, R., VIBOL, U., KERR, S. J., KANJANAVANIT, S., NGAMPIYASKUL, C., WONGSAWAT, J., LUESOMBOON, W., NGO-GIANG-HUONG, N., CHETTRA, K., CHEUNYAM, T., SUWARNLERK, T., UBOLYAM, S., SHEARER, W. T., PAUL, R., MOFENSON, L. M., FOX, L., LAW, M. G., COOPER, D. A., PHANUPHAK, P., VUN, M. C., RUXRUNGTHAM, K. & GROUP, P. S. 2012. Early versus deferred antiretroviral therapy for children older than 1 year infected with HIV (PREDICT): a multicentre, randomised, open-label trial. *Lancet Infect Dis,* 12**,** 933-41.

RANDALL, S. R., WARTON, C. M. R., HOLMES, M. J., COTTON, M. F., LAUGHTON, B., VAN DER KOUWE, A. J. W. & MEINTJES, E. M. 2017. Larger Subcortical Gray Matter Structures and Smaller Corpora Callosa at Age 5 Years in HIV Infected Children on Early ART. *Front Neuroanat,* 11**,** 95.

REHMAN, A. & AL KHALILI, Y. 2023. Neuroanatomy, Occipital Lobe. *StatPearls.* Treasure Island (FL).

REYNOLDS, L. M. & FLORES, C. 2021. Mesocorticolimbic Dopamine Pathways Across Adolescence: Diversity in Development. *Front Neural Circuits,* 15**,** 735625.

ROBERTSON, F. C., HOLMES, M. J., COTTON, M. F., DOBBELS, E., LITTLE, F., LAUGHTON, B., VAN DER KOUWE, A. J. W. & MEINTJES, E. M. 2018. Perinatal HIV Infection or Exposure Is Associated With Low N-Acetylaspartate and Glutamate in Basal Ganglia at Age 9 but Not 7 Years. *Front Hum Neurosci,* 12**,** 145.

ROLLS, E. T. 2004. The functions of the orbitofrontal cortex. *Brain Cogn,* 55**,** 11-29.

RUEL, T. D., BOIVIN, M. J., BOAL, H. E., BANGIRANA, P., CHARLEBOIS, E., HAVLIR, D. V., ROSENTHAL, P. J., DORSEY, G., ACHAN, J., AKELLO, C., KAMYA, M. R. & WONG, J. K. 2012. Neurocognitive and motor deficits in HIV-infected Ugandan children with high CD4 cell counts. *Clin Infect Dis,* 54**,** 1001-9.

SINAI, I. S. O. M. A. M. 2018. *Brain Reward Pathways* [Online]. Available: http://neuroscience.mssm.edu/nestler/nidappg/brain_reward_pathways.html [Accessed].

SOMERVILLE, L. H., BOOKHEIMER, S. Y., BUCKNER, R. L., BURGESS, G. C., CURTISS, S. W., DAPRETTO, M., ELAM, J. S., GAFFREY, M. S., HARMS, M. P., HODGE, C., KANDALA, S., KASTMAN, E. K., NICHOLS, T. E., SCHLAGGAR, B. L., SMITH, S. M., THOMAS, K. M., YACOUB, E., VAN ESSEN, D. C. & BARCH, D.

M. 2018. The Lifespan Human Connectome Project in Development: A large-scale study of brain connectivity development in 5-21 year olds. *Neuroimage,* 183**,** 456-468.
SOMERVILLE, L. H., HARE, T. & CASEY, B. J. 2011. Frontostriatal maturation predicts cognitive control failure to appetitive cues in adolescents. *J Cogn Neurosci,* 23**,** 2123-34.
SOWELL, E. R., TRAUNER, D. A., GAMST, A. & JERNIGAN, T. L. 2002. Development of cortical and subcortical brain structures in childhood and adolescence: a structural MRI study. *Dev Med Child Neurol,* 44**,** 4-16.
TELZER, E. H. 2016. Dopaminergic reward sensitivity can promote adolescent health: A new perspective on the mechanism of ventral striatum activation. *Dev Cogn Neurosci,* 17**,** 57-67.
TELZER, E. H., FULIGNI, A. J., LIEBERMAN, M. D. & GALVAN, A. 2013. Meaningful family relationships: neurocognitive buffers of adolescent risk taking. *J Cogn Neurosci,* 25**,** 374-87.
TOGA, A. W., THOMPSON, P. M. & SOWELL, E. R. 2006. Mapping brain maturation. *Trends Neurosci,* 29**,** 148-59.
UDDIN, L. Q., NOMI, J. S., HEBERT-SEROPIAN, B., GHAZIRI, J. & BOUCHER, O. 2017. Structure and Function of the Human Insula. *J Clin Neurophysiol,* 34**,** 300-306.
UNAIDS. 2021a. *Country Factsheets: South Africa* [Online]. Available: https://aidsinfo.unaids.org/ [Accessed].
UNAIDS. 2021b. *Global HIV & AIDS statistics - Fact sheet* [Online]. Available: https://www.unaids.org/en/resources/fact-sheet [Accessed].
UNAIDS. 2021c. *Regional Fact Sheet - Eastern and Southern Africa* [Online]. Available: https://aidsinfo.unaids.org/ [Accessed].
UNAIDS. 2021d. *UNAIDS Dashboard* [Online]. Available: https://kpatlas.unaids.org/dashboard [Accessed].
VAN LEIJENHORST, L., GUNTHER MOOR, B., OP DE MACKS, Z. A., ROMBOUTS, S. A., WESTENBERG, P. M. & CRONE, E. A. 2010a. Adolescent risky decision-making: neurocognitive development of reward and control regions. *Neuroimage,* 51**,** 345-55.
VAN LEIJENHORST, L., ZANOLIE, K., VAN MEEL, C. S., WESTENBERG, P. M., ROMBOUTS, S. A. & CRONE, E. A. 2010b. What motivates the adolescent? Brain regions mediating reward sensitivity across adolescence. *Cereb Cortex,* 20**,** 61-9.
VAN WYHE, K. S., LAUGHTON, B., COTTON, M. F., MEINTJES, E. M., VAN DER KOUWE, A. J., BOIVIN, M. J., KIDD, M. & THOMAS, K. G. 2021. Cognitive outcomes at ages seven and nine years in South African children from the children with HIV early antiretroviral (CHER) trial: a longitudinal investigation. *J Int AIDS Soc,* 24**,** e25734.
WANG, K. S., SMITH, D. V. & DELGADO, M. R. 2016. Using fMRI to study reward processing in humans: past, present, and future. *J Neurophysiol,* 115**,** 1664-78.
WHO. 2010. *SEXUAL MATURITY RATING (TANNER STAGING) IN ADOLESCENTS* [Online]. Available: https://www.ncbi.nlm.nih.gov/books/NBK138588/ [Accessed].
WOOLRICH, M. W., BEHRENS, T. E., BECKMANN, C. F., JENKINSON, M. & SMITH, S. M. 2004. Multilevel linear modelling for FMRI group analysis using Bayesian inference. *Neuroimage,* 21**,** 1732-47.
WOOLRICH, M. W., RIPLEY, B. D., BRADY, M. & SMITH, S. M. 2001. Temporal autocorrelation in univariate linear modeling of FMRI data. *Neuroimage,* 14**,** 1370-86.
XU, J., MOELLER, S., AUERBACH, E. J., STRUPP, J., SMITH, S. M., FEINBERG, D. A., YACOUB, E. & UGURBIL, K. 2013. Evaluation of slice accelerations using multiband echo planar imaging at 3 T. *Neuroimage,* 83**,** 991-1001.
YANG, S., BOUDIER-REVERET, M., CHOO, Y. J. & CHANG, M. C. 2020. Association between Chronic Pain and Alterations in the Mesolimbic Dopaminergic System. *Brain Sci,* 10.

APPENDIX A

Results included in this manuscript come from preprocessing performed using fMRIPrep 21.0.1 (Esteban, Markiewicz, et al. (2018); Esteban, Blair, et al. (2018); RRID:SCR_016216), which is based on Nipype 1.6.1 (K. Gorgolewski et al. (2011); K. J. Gorgolewski et al. (2018); RRID:SCR_002502).

Anatomical data preprocessing:

A total of 1 T1-weighted (T1w) images were found within the input BIDS dataset. The T1-weighted (T1w) image was corrected for intensity non-uniformity (INU) with N4BiasFieldCorrection (Tustison et al. 2010), distributed with ANTs 2.3.3 (Avants et al. 2008, RRID:SCR_004757), and used as T1w-reference throughout the workflow. The T1w-reference was then skull-stripped with a Nipype implementation of the antsBrainExtraction.sh workflow (from ANTs), using OASIS30ANTs as target template. Brain tissue segmentation of cerebrospinal fluid (CSF), white-matter (WM) and gray-matter (GM) was performed on the brain-extracted T1w using fast (FSL 6.0.5.1:57b01774, RRID:SCR_002823, Zhang, Brady, and Smith 2001). Brain surfaces were reconstructed using recon-all (FreeSurfer 6.0.1, RRID:SCR_001847, Dale, Fischl, and Sereno 1999), and the brain mask estimated previously was refined with a custom variation of the method to reconcile ANTs-derived and FreeSurfer-derived segmentations of the cortical gray-matter of Mindboggle (RRID:SCR_002438, Klein et al. 2017). Volume-based spatial normalization to two standard spaces (MNI152NLin6Asym, MNI152NLin2009cAsym) was performed through nonlinear registration with antsRegistration (ANTs 2.3.3), using brain-extracted versions of both T1w reference and the T1w template. The following templates were selected for spatial normalization: FSL's MNI ICBM 152 non-linear 6th Generation Asymmetric Average Brain Stereotaxic Registration Model [Evans et al. (2012), RRID:SCR_002823; TemplateFlow ID: MNI152NLin6Asym], ICBM 152 Nonlinear Asymmetrical template version 2009c [Fonov et al. (2009), RRID:SCR_008796; TemplateFlow ID: MNI152NLin2009cAsym].

Functional data preprocessing:

First, a reference volume and its skull-stripped version were generated by aligning and averaging 1 single-band references (SBRefs). Head-motion parameters with respect to the BOLD reference (transformation matrices, and six corresponding rotation and translation parameters) are estimated before any spatiotemporal filtering using mcflirt (FSL 6.0.5.1:57b01774, Jenkinson et al. 2002). BOLD runs were slice-time corrected to 0.365s (0.5 of slice acquisition range 0s-0.73s) using 3dTshift from AFNI (Cox and Hyde 1997, RRID:SCR_005927). The BOLD time-series (including slice-timing correction when applied) were resampled onto their original, native space by applying the transforms to correct for head-motion. These resampled BOLD time-series will be referred to as preprocessed BOLD in original space, or just preprocessed BOLD. The BOLD reference was then co-registered to the T1w reference using bbregister (FreeSurfer) which implements boundary-based registration (Greve and Fischl 2009). Co-registration was configured with six degrees of freedom. First, a reference volume and its skull-stripped version were generated using a custom methodology of fMRIPrep. Several confounding time-series were

calculated based on the preprocessed BOLD: framewise displacement (FD), DVARS and three region-wise global signals. FD was computed using two formulations following Power (absolute sum of relative motions, Power et al. (2014)) and Jenkinson (relative root mean square displacement between affines, Jenkinson et al. (2002)). FD and DVARS are calculated for each functional run, both using their implementations in Nipype (following the definitions by Power et al. 2014). The three global signals are extracted within the CSF, the WM, and the whole-brain masks. Additionally, a set of physiological regressors were extracted to allow for component-based noise correction (CompCor, Behzadi et al. 2007). Principal components are estimated after high-pass filtering the preprocessed BOLD time-series (using a discrete cosine filter with 128s cut-off) for the two CompCor variants: temporal (tCompCor) and anatomical (aCompCor). tCompCor components are then calculated from the top 2% variable voxels within the brain mask. For aCompCor, three probabilistic masks (CSF, WM and combined CSF+WM) are generated in anatomical space. The implementation differs from that of Behzadi et al. in that instead of eroding the masks by 2 pixels on BOLD space, the aCompCor masks are subtracted a mask of pixels that likely contain a volume fraction of GM. This mask is obtained by dilating a GM mask extracted from the FreeSurfer's aseg segmentation, and it ensures components are not extracted from voxels containing a minimal fraction of GM. Finally, these masks are resampled into BOLD space and binarized by thresholding at 0.99 (as in the original implementation). Components are also calculated separately within the WM and CSF masks. For each CompCor decomposition, the k components with the largest singular values are retained, such that the retained components' time series are sufficient to explain 50 percent of variance across the nuisance mask (CSF, WM, combined, or temporal). The remaining components are dropped from consideration. The head-motion estimates calculated in the correction step were also placed within the corresponding confounds file. The confound time series derived from head motion estimates and global signals were expanded with the inclusion of temporal derivatives and quadratic terms for each (Satterthwaite et al. 2013). Frames that exceeded a threshold of 0.5 mm FD or 1.5 standardised DVARS were annotated as motion outliers. The BOLD time-series were resampled into several standard spaces, correspondingly generating the following spatially-normalized, preprocessed BOLD runs: MNI152NLin6Asym, MNI152NLin2009cAsym. First, a reference volume and its skull-stripped version were generated using a custom methodology of fMRIPrep. All resamplings can be performed with a single interpolation step by composing all the pertinent transformations (i.e. head-motion transform matrices, susceptibility distortion correction when available, and co-registrations to anatomical and output spaces). Gridded (volumetric) resamplings were performed using antsApplyTransforms (ANTs), configured with Lanczos interpolation to minimize the smoothing effects of other kernels (Lanczos 1964). Non-gridded (surface) resamplings were performed using mri_vol2surf (FreeSurfer).

APPENDIX B

H1: Whole Group	Max X;Y;Z (MNI,mm)	Number of Voxels	Voxels (mm3)
Lateral Occipital Cortex, superior division: 9% **Lateral Occipital Cortex, inferior division: 6%** **Lingual Gyrus: 6%** **Occipital Pole: 9%**	-26.9; -62.9; -8.9	18064	249716.736
R Middle Frontal Gyrus: 22% **R Precentral Gyrus: 10%**	35.5; 9.1; 31.9	1670	23086.08
Left Middle Frontal Gyrus: 19% **Left Precentral Gyrus: 17%**	-41.3; -0.5; 36.7	1448	20017.152
Right Insular Cortex: 16%	33.1; 18.7; -4.1	563	7782.912
Left Insular Cortex: 14%	-29.3; 18.7; -6.5	486	6718.464
Superior Frontal Gyrus: 16% **Paracingulate Gyrus: 29%**	-5.3; 11.5; 53.5	481	6649.344
Superior Temporal Gyrus, posterior division: 24% **Middle Temporal Gyrus, posterior division: 20%**	-55.7; -41.3; 0.7	219	3027.456
Left Crus II: 44% **Left VIIb: 50%**	-29.3; -72.5; -49.7	59	815.616
Cingulate Gyrus, anterior division: 40%	4.3; 1.9; 29.5	58	801.792
Right VIIb: 59% **Right VIIIa: 33%**	30.7; -65.3; -54.5	44	608.256
Vermis IX: 44% **Vermis X: 21%**	-0.5; -50.9; -35.3	30	414.72
Frontal Pole: 36% **Inferior Frontal Gyrus, pars triangularis: 21%**	-53.3; 37.9; -1.7	22	304.128

H1: CPHIV	Max X;Y;Z (MNI,mm)	Number of Voxels	Voxels mm3
Lateral Occipital Cortex, superior division: 9% **Lateral Occipital Cortex, inferior division: 8%** **Lingual Gyrus: 6%** **Occipital Fusiform Gyrus: 6%** **Occipital Pole: 11%**	30.7; -84.5; -13.7	12584	173961.2
R Middle Frontal Gyrus: 24% **R Precentral Gyrus: 10%**	35.5; 9.1; 31.9	1021	14114.3
L Middle Frontal Gyrus: 20% **L Precentral Gyrus: 17%**	-41.3; -0.5; 36.7	991	13699.58
R Insular Cortex: 26% **R Frontal Orbital Cortex: 21%**	35.5; 21.1; -4.1	243	3359.232

L Superior Temporal Gyrus, posterior division: 28% **L Middle Temporal Gyrus, posterior division: 21%**	-53.3; -36.5; 5.5	126	1741.824
Left Cerebral White Matter: 28% **Left Thalamus: 32%**	-19.7; -29.3; -4.1	119	1645.056
L Insular Cortex: 29% **L Frontal Orbital Cortex: 12%**	-29.3; 18.7; -6.5	107	1479.168
Right Thalamus: 95%	11.5; -12.5; 10.3	105	1451.52
Right Cerebral White Matter: 32% **Right Caudate: 43%**	9.1; 6.7; 0.7	100	1382.4
Right Cerebral White Matter: 28% **Right Thalamus: 42%**	23.5; -26.9; -4.1	72	995.328
R Superior Temporal Gyrus, posterior division: 29% **R Middle Temporal Gyrus, posterior division: 25%**	47.5; -31.7; -1.7	58	801.792
R Superior Frontal Gyrus: 16% **R Paracingulate Gyrus: 19%**	-5.3; 11.5; 53.5	54	746.496
R Frontal Pole: 37% **R Frontal Orbital Cortex: 28%**	23.5; 33.1; -11.3	26	359.424
Left Cerebral White Matter: 55% **Left Caudate: 41%**	-17.3; 16.3; 3.1	26	359.424
Left Thalamus: 93%	-12.5; -14.9; 5.5	24	331.776
L Superior Frontal Gyrus: 25% **L Paracingulate Gyrus: 44%**	4.3; 13.9; 48.7	22	304.128

H1: Controls	Max X;Y;Z (MNI,mm)	Number of Voxels	Voxels mm3
Lateral Occipital Cortex, superior division: 10% **Lateral Occipital Cortex, inferior division: 7%** **Lingual Gyrus: 6%** **Occipital Pole: 10%**	28.3; -77.3; -11.3	15160	209571.8
R Middle Frontal Gyrus: 23% **R Precentral Gyrus: 10%**	42.7; 11.5; 27.1	1243	17183.23
L Middle Frontal Gyrus: 19% **L Precentral Gyrus: 18%**	-50.9; 11.5; 31.9	998	13796.35
Superior Frontal Gyrus: 13% **Paracingulate Gyrus: 33%** **Cingulate Gyrus, anterior division: 10%**	4.3; 13.9; 53.5	424	5861.376
Right Thalamus: 35% **Right Caudate: 12%**	-19.7; -29.3; -4.1	343	4741.632
R Insular Cortex: 24% **R Frontal Orbital Cortex: 18%**	35.5; 18.7; 3.1	314	4340.736

L Insular Cortex: 29% **L Frontal Orbital Cortex: 13%** **L Frontal Operculum Cortex: 13%**	-29.3; 25.9; 3.1	203	2806.272
L Superior Temporal Gyrus, posterior division: 24% **L Middle Temporal Gyrus, posterior division: 20%**	-55.7; -41.3; 0.7	92	1271.808
Left Cerebral White Matter: 45% **Left Caudate: 25%** **Left Putamen: 23%**	-17.3; 9.1; 0.7	68	940.032
R Frontal Pole: 47% **R Frontal Orbital Cortex: 23%**	21.1; 33.1; -16.1	64	884.736
Cingulate Gyrus, anterior division: 37%	4.3; -2.9; 31.9	59	815.616
Left Thalamus: 98%	-10.1; -12.5; 7.9	51	705.024
Left Crus II: 63% **Left VIIb: 31%**	-29.3; -72.5; -47.3	49	677.376
L Temporal Pole: 34%	-48.5; 21.1; -13.7	37	511.488
Left Cerebral White Matter: 24% **Left Caudate: 73%**	-12.5; 6.7; 12.7	33	456.192
Right Crus II: 19% **Right VIIb: 64%** **Right VIIIa: 13%**	23.5; -74.9; -47.3	26	359.424

No activated clusters for H1: CPHIV>Controls

H1: CPHIV<Controls	Max X;Y;Z (MNI,mm)	Number of Voxels	Voxels mm3
L Occipital Pole: 52%	-17.3; -101; 3.1	62	857.088
L Temporal Pole: 18% **L Frontal Orbital Cortex: 28%**	-46.1; 16.3; -8.9	23	317.952
Paracingulate Gyrus: 57% **Cingulate Gyrus, anterior division: 22%**	-0.5; 21.1; 36.7	22	304.128

H2: Whole Group	Max X;Y;Z (MNI,mm)	Number of Voxels	Voxels mm3
L + R Lateral Occipital Cortex, superior division: 14% **L + R Occipital Pole: 11%**	-12.5; -96.5; 3.1	6970	96353.28
L + R Cerebral White Matter: 29% **L Putamen: 11%** **R Cerebral Cortex: 14%** **R Putamen: 12%**	-10.1; 9.1; 0.7	2793	38610.43

R Frontal Pole: 10% **R Middle Frontal Gyrus: 15%** **R Precentral Gyrus: 15%**	47.5; 9.1; 22.3	1603	22159.87
L Frontal Pole: 8% **L Middle Frontal Gyrus: 16%** **L Precentral Gyrus: 16%**	-48.5; 35.5; 27.1	962	13298.69
L + R Superior Frontal Gyrus: 5% **L + R Paracingulate Gyrus: 33%** **L + R Cingulate Gyrus, anterior division: 25%**	-5.3; 25.9; 41.5	816	11280.38
R Middle and Inferior Temporal Gyrus, temporooccipital part: 37% **R Lateral Occipital Cortex, inferior division: 14%**	54.7; -55.7; -13.7	495	6842.88
L + R Cingulate Gyrus, anterior and posterior division: 54%	-2.9; -31.7; 29.5	410	5667.84
R Crus I: 52% **R Crus II: 24%**	40.3; -65.3; -42.5	358	4948.992
L Superior Parietal Lobule: 16% **L Supramarginal Gyrus, anterior and posterior division: 31%**	-48.5; -43.7; 51.1	310	4285.44
L Frontal Pole: 32% **L Frontal Orbital Cortex: 41%**	-24.5; 33.1; -13.7	114	1575.936
R Frontal Pole: 52%	28.3; 57.1; -8.9	60	829.44
R Crus II: 27% **R VIIb: 54%**	25.9; -67.7; -47.3	57	787.968
R Parahippocampal Gyrus, posterior division: 29% **R Temporal Fusiform Cortex, posterior division: 31%** **R Temporal Occipital Fusiform Cortex: 12%**	25.9; -38.9; -18.5	30	414.72
R Frontal Pole: 68%	37.9; 61.9; 7.9	30	414.72
R Intracalcarine Cortex: 31%	16.3; -74.9; 12.7	25	345.6
R Temporal Occipital Fusiform Cortex: 65%	33.1; -50.9; -18.5	24	331.776
R Cingulate Gyrus, posterior division: 21% **R Precuneus Cortex: 13%**	6.7; -43.7; 12.7	24	331.776

H2: CPHIV	Max X;Y;Z (MNI,mm)	Number of Voxels	Voxels mm3
Lateral Occipital Cortex, superior division: 4% **Lateral Occipital Cortex, inferior division: 5%** **Occipital Pole: 17%**	-19.7; -98.9; 24.7	1629	22519.3
Left Cerebral White Matter: 15% **Left Putamen: 24%** **Right Putamen: 22%**	-12.5; 4.3; -8.9	747	10326.53

R Middle Frontal Gyrus: 15% **R Inferior Frontal Gyrus, pars opercularis: 16%** **R Precentral Gyrus: 19%**	45.1; 6.7; 24.7	481	6649.344
R Lateral Occipital Cortex, superior division: 38%	28.3; -65.3; 43.9	396	5474.304
L Lateral Occipital Cortex, superior division: 50%	-22.1; -67.7; 41.5	286	3953.664
R Middle Temporal Gyrus, temporooccipital part: 23% **R Inferior Temporal Gyrus, temporooccipital part: 32%**	59.5; -50.9; -8.9	189	2612.736
Occipital Pole: 55%	16.3; -94.1; 5.5	175	2419.2
Cingulate Gyrus, posterior division: 71%	-2.9; -31.7; 29.5	100	1382.4
Right Crus I: 27% **Right Crus II: 56%**	37.9; -65.3; -42.5	99	1368.576
L Middle Frontal Gyrus: 15% **L Precentral Gyrus: 33%**	-41.3; 1.9; 31.9	95	1313.28
R Frontal Pole: 41% **R Frontal Orbital Cortex: 34%**	23.5; 28.3; -16.1	71	981.504
Paracingulate Gyrus: 30% **Cingulate Gyrus, anterior division: 47%**	6.7; 40.3; -6.5	66	912.384
R Frontal Pole: 26% **R Middle Frontal Gyrus: 17%**	54.7; 33.1; 24.7	64	884.736
R Insular Cortex: 24% **R Frontal Orbital Cortex: 24%**	35.5; 25.9; 0.7	55	760.32
R Lateral Occipital Cortex, inferior division: 54% **R Occipital Pole: 13%**	45.1; -82.1; -1.7	53	732.672
L Middle Temporal Gyrus, temporooccipital part: 11% **L Inferior Temporal Gyrus, temporooccipital part: 39%** **L Lateral Occipital Cortex, inferior division: 17%**	-53.3; -60.5; -11.3	52	718.848
L Frontal Pole: 14% **L Middle Frontal Gyrus: 30%**	-48.5; 35.5; 27.1	43	594.432
L Superior Parietal Lobule: 37%	-29.3; -50.9; 48.7	36	497.664
L Supramarginal Gyrus, anterior division: 28% **L Supramarginal Gyrus, posterior division: 28%**	-48.5; -41.3; 51.1	33	456.192
R Occipital Pole: 50%	25.9; -96.5; -4.1	30	414.72
L Temporal Occipital Fusiform Cortex: 58%	-34.1; -48.5; -18.5	27	373.248
Right VI: 22% **Right Crus I: 72%**	35.5; -58.1; -32.9	24	331.776

H2: Controls	Max X;Y;Z (MNI,mm)	Number of Voxels	Voxels mm3
Left Cerebral White Matter: 12% **Left Caudate: 7%** **Left Putamen: 17%** **Right Cerebral White Matter: 15%** **Right Cerebral Cortex: 10%** **Right Caudate: 7%** **Right Putamen: 13%**	18.7; 6.7; 0.7	1425	19699.2
L Middle Frontal Gyrus: 18% **L Precentral Gyrus: 19%**	-41.3; -2.9; 51.1	571	7893.504
L Superior Frontal Gyrus: 8% **L Paracingulate Gyrus: 31%** **L Cingulate Gyrus, anterior division: 22%**	-10.1; 21.1; 46.3	557	7699.968
Occipital Pole: 31%	-7.7; -98.9; -4.1	473	6538.752
Lingual Gyrus: 11% **Occipital Fusiform Gyrus: 11%** **Occipital Pole: 28%**	16.3; -91.7; 5.5	268	3704.832
L Superior Frontal Gyrus: 26% **L Middle Frontal Gyrus: 17%**	-26.9; 13.9; 65.5	210	2903.04
R Middle Frontal Gyrus: 9% **R Inferior Frontal Gyrus, pars opercularis: 23%** **R Precentral Gyrus: 21%**	35.5; 4.3; 36.7	196	2709.504
R Middle Frontal Gyrus: 15% **R Precentral Gyrus: 35%**	35.5; -5.3; 53.5	153	2115.072
R Lateral Occipital Cortex, superior division: 49%	33.1; -67.7; 24.7	104	1437.696
Left VI: 25% **Left Crus I: 21%** **Left Crus II: 35%**	-22.1; -60.5; -32.9	97	1340.928
L Frontal Pole: 29% **L Frontal Orbital Cortex: 38%**	-24.5; 33.1; -13.7	84	1161.216
L Lateral Occipital Cortex, superior division: 44%	-19.7; -62.9; 41.5	76	1050.624
L Insular Cortex: 19% **L Frontal Orbital Cortex: 14%** **L Frontal Operculum Cortex: 24%**	-31.7; 28.3; 3.1	72	995.328
L Supramarginal Gyrus, anterior division: 17% **L Supramarginal Gyrus, posterior division: 24%**	-53.3; -38.9; 43.9	65	898.56
Right Crus I: 75%	42.7; -62.9; -37.7	56	774.144
R Inferior Temporal Gyrus, temporooccipital part: 43%	49.9; -53.3; -11.3	56	774.144

L Lateral Occipital Cortex, superior division: 7% **L Occipital Pole: 45%**	-29.3; -94.1; 22.3	50	691.2
Left Crus I: 83%	-38.9; -74.9; -28.1	50	691.2
L Middle Temporal Gyrus, temporooccipital part: 7% **L Inferior Temporal Gyrus, temporooccipital part: 42%** **L Lateral Occipital Cortex, inferior division: 12%**	-53.3; -60.5; -11.3	49	677.376
R Superior Frontal Gyrus: 31% **R Middle Frontal Gyrus: 18%**	23.5; 18.7; 63.1	44	608.256
Cingulate Gyrus, anterior division: 48% **Cingulate Gyrus, posterior division: 12%**	-0.5; -14.9; 34.3	38	525.312
L Lateral Occipital Cortex, inferior division: 40% **L Occipital Fusiform Gyrus: 22%**	-34.1; -79.7; -13.7	35	483.84
L Frontal Medial Cortex: 12% **L Paracingulate Gyrus: 25%**	-12.5; 40.3; -6.5	35	483.84
Cingulate Gyrus, anterior division: 37%	-2.9; 4.3; 29.5	28	387.072
R Superior Parietal Lobule: 33%	18.7; -55.7; 53.5	26	359.424
Vermis IX: 33% **Vermis X: 13%**	1.9; -53.3; -35.3	26	359.424

No activated clusters for H2: CPHIV>Controls

H2: CPHIV<Controls	Max X;Y;Z (MNI,mm)	Number of Voxels	Voxels mm3
L Superior and Middle Frontal Gyrus: 36%	-19.7; 25.9; 39.1	24	331.776

H3a: Whole Group	Max X;Y;Z (MNI,mm)	Number of Voxels	Voxels mm3
Left Cerebral Cortex: 21% **Right Cerebral Cortex: 34%**	-19.7; -29.3; 22.3	24302	335950.848
L Temporal Fusiform Cortex, posterior division: 35% **L Temporal Occipital Fusiform Cortex: 22%**	-22.1; -48.5; -16.1	197	2723.328
Occipital Pole: 16%	-0.5; -94.1; 17.5	124	1714.176
L Supramarginal Gyrus, anterior division: 23% **L Supramarginal Gyrus, posterior division: 7%**	-60.5; -38.9; 51.1	76	1050.624
Left IX: 12% **Vermis X: 6%**	-5.3; -46.1; -35.3	71	981.504
R Parahippocampal Gyrus, posterior division: 20% **R Lingual Gyrus: 9%** **R Temporal Fusiform Cortex, posterior division: 12%** **R Temporal Occipital Fusiform Cortex: 27%**	33.1; -36.5; -11.3	70	967.68

L Precuneus Cortex: 40% **L Supracalcarine Cortex: 11%**	-12.5; -60.5; 17.5	65	898.56
R Parahippocampal Gyrus, anterior division: 30% **R Temporal Fusiform Cortex, posterior division: 27%**	37.9; -10.1; -28.1	51	705.024
Left VIIIb: 4% **Left IX: 40%** **Left X: 6%**	-12.5; -43.7; -44.9	35	483.84
L Intracalcarine Cortex: 18%	-19.7; -74.9; 5.5	27	373.248
R Inferior Temporal Gyrus, posterior division: 42%	52.3; -29.3; -28.1	27	373.248
Cingulate Gyrus, anterior division: 69% **Cingulate Gyrus, posterior division: 6%**	-0.5; -10.1; 31.9	26	359.424
L Superior Frontal Gyrus: 6% **L Middle Frontal Gyrus: 27%**	-29.3; 13.9; 48.7	25	345.6

H3a: CPHIV	**Max X;Y;Z (MNI,mm)**	**Number of Voxels**	**Voxels mm3**
L Frontal Pole: 10% **L Precentral Gyrus: 7%** **L Postcentral Gyrus: 5%**	-17.3; -14.9; 77.5	5514	76225.54
Left Cerebral White Matter: 13% **Left Lateral Ventricle: 26%** **Right Cerebral White Matter: 12%** **Right Lateral Ventricle: 27%**	-19.7; -29.3; 22.3	1477	20418.05
L Frontal Pole: 45% **L Middle Frontal Gyrus: 10%**	-36.5; 42.7; 36.7	380	5253.12
L Supramarginal Gyrus, posterior division: 20% **L Angular Gyrus: 21%**	-58.1; -46.1; 7.9	153	2115.072
Left V: 16% **Right V: 11%** **Left VI: 12%** **Vermis VI: 26%**	-2.9; -77.3; -23.3	122	1686.528
L Insular Cortex: 23% **L Temporal Pole: 6%** **L Frontal Orbital Cortex: 9%** **L Frontal Operculum Cortex: 8%**	-41.3; 13.9; -11.3	75	1036.8
L Inferior Frontal Gyrus, pars opercularis: 15% **L Precentral Gyrus: 8%**	-67.7; -7.7; 12.7	73	1009.152
R Lateral Occipital Cortex, superior division: 66%	45.1; -67.7; 31.9	62	857.088
R Precentral Gyrus: 42% **R Postcentral Gyrus: 22%**	42.7; -12.5; 51.1	60	829.44
L Inferior Frontal Gyrus, pars opercularis: 17% **L Precentral Gyrus: 11%**	-62.9; 11.5; 17.5	58	801.792

R Middle Temporal Gyrus, temporooccipital part: 36% **R Lateral Occipital Cortex, inferior division: 33%**	59.5; -65.3; 0.7	54	746.496
L Central Opercular Cortex: 16% **L Planum Polare: 30%**	-48.5; -2.9; 0.7	42	580.608
Precuneus Cortex: 53% **Cuneal Cortex: 14%**	1.9; -72.5; 41.5	42	580.608
L Superior Frontal Gyrus: 21% **L Middle Frontal Gyrus: 12%**	-29.3; -0.5; 67.9	38	525.312
L Lateral Occipital Cortex, superior division: 27% **L Lateral Occipital Cortex, inferior division: 34%**	-55.7; -67.7; 12.7	36	497.664
Occipital Pole: 51%	-12.5; -106; -4.1	35	483.84
L Supramarginal Gyrus, anterior division: 31%	-58.1; -26.9; 53.5	33	456.192
L Occipital Fusiform Gyrus: 21% **L Occipital Pole: 22%**	-17.3; -91.7; -16.1	30	414.72
Frontal Pole: 54%	-17.3; 61.9; 27.1	28	387.072
R Precentral Gyrus: 12% **R Postcentral Gyrus: 23%** **R Central Opercular Cortex: 23%**	61.9; -12.5; 15.1	27	373.248
Left Crus I: 29% **Left Crus II: 64%**	-38.9; -74.9; -40.1	27	373.248
L Occipital Pole: 49%	-26.9; -101; 12.7	27	373.248
L Lateral Occipital Cortex, superior division: 64%	-43.7; -82.1; 27.1	26	359.424
R Superior Temporal Gyrus, posterior division: 34% **R Middle Temporal Gyrus, posterior division: 38%**	54.7; -22.1; -4.1	26	359.424
L Superior Temporal Gyrus, posterior division: 34%	-67.7; -19.7; 3.1	25	345.6
L Middle Frontal Gyrus: 19%	-58.1; 18.7; 31.9	24	331.776
L Superior Frontal Gyrus: 20% **L Middle Frontal Gyrus: 27%**	-29.3; 16.3; 60.7	23	317.952

H3a: Controls	Max X;Y;Z (MNI,mm)	Number of Voxels	Voxels mm3
R Frontal Pole: 7% **R Superior Frontal Gyrus: 7%** **R Middle Frontal Gyrus: 6%** **R Paracingulate Gyrus: 7%** **R Precuneus Cortex: 10%**	49.9; 9.1; 48.7	3433	47457.79
Left Crus I: 27% **Left Crus II: 22%**	-12.5; -82.1; -44.9	1606	22201.34

R Angular Gyrus: 14% **R Lateral Occipital Cortex, superior division: 15%**	61.9; -50.9; 5.5	1412	19519.49
Left Lateral Ventricle: 23% **Right Lateral Ventricle: 25%**	4.3; 9.1; 12.7	849	11736.58
R Frontal Pole: 12% **R Frontal Orbital Cortex: 19%**	45.1; 21.1; -11.3	415	5736.96
L Superior Temporal Gyrus, posterior division: 16% **L Middle Temporal Gyrus, posterior division: 9%** **L Supramarginal Gyrus, posterior division: 14%** **L Angular Gyrus: 12%** **L Planum Temporale: 10%**	-62.9; -43.7; 22.3	264	3649.536
R Lateral Occipital Cortex, inferior division: 7% **R Occipital Fusiform Gyrus: 17%** **R Occipital Pole: 8%**	30.7; -74.9; -13.7	209	2889.216
L Insular Cortex: 6% **L Frontal Orbital Cortex: 19%**	-46.1; 16.3; -8.9	199	2750.976
R Frontal Pole: 56%	49.9; 49.9; -1.7	139	1921.536
R Cingulate Gyrus, posterior division: 10% **R Lingual Gyrus: 8%**	11.5; -41.3; 0.7	118	1631.232
L Lateral Occipital Cortex, superior division: 33% **L Lateral Occipital Cortex, inferior division: 27%**	-50.9; -62.9; 10.3	99	1368.576
Right Crus I: 31% **Right Crus II: 40%**	28.3; -82.1; -44.9	86	1188.864
L Middle Frontal Gyrus: 18% **L Precentral Gyrus: 15%**	-55.7; -2.9; 51.1	85	1175.04
L Lateral Occipital Cortex, superior division: 57% **L Occipital Pole: 11%**	-26.9; -84.5; 31.9	82	1133.568
L Insular Cortex: 10% **L Planum Polare: 22%** **L Heschl's Gyrus (includes H1 and H2): 10%**	-50.9; -10.1; 0.7	79	1092.096
L Lingual Gyrus: 31% **L Temporal Occipital Fusiform Cortex: 30%**	-26.9; -46.1; -6.5	71	981.504
Cuneal Cortex: 15% **Occipital Pole: 40%**	-7.7; -89.3; 19.9	66	912.384
Left VIIIb: 29% **Left IX: 47%**	-5.3; -58.1; -47.3	64	884.736
L Lateral Occipital Cortex, superior division: 6% **L Lateral Occipital Cortex, inferior division: 68%**	-46.1; -74.9; 5.5	44	608.256
R Temporal Pole: 23% **R Middle Temporal Gyrus, anterior division: 14%**	61.9; 4.3; -30.5	43	594.432
L Frontal Pole: 69%	-17.3; 69.1; 15.1	41	566.784

L Temporal Pole: 49% **L Superior Temporal Gyrus, anterior division: 10%**	-50.9; 6.7; -28.1	40	552.96
R Parahippocampal Gyrus, posterior division: 33% **R Lingual Gyrus: 17%**	30.7; -36.5; -11.3	39	539.136
R Inferior Temporal Gyrus, posterior division: 24% **R Temporal Fusiform Cortex, posterior division: 19%**	40.3; -10.1; -32.9	38	525.312
R Superior Temporal Gyrus, posterior division: 18% **R Parietal Operculum Cortex: 22%** **R Planum Temporale: 24%**	57.1; -29.3; 22.3	35	483.84
R Frontal Pole: 63%	37.9; 64.3; 5.5	34	470.016
R Middle Temporal Gyrus, posterior division: 9% **R Inferior Temporal Gyrus, posterior division: 39%**	57.1; -26.9; -30.5	32	442.368
Lateral Occipital Cortex, superior division: 36% **Precuneus Cortex: 13%**	-10.1; -84.5; 43.9	31	428.544
Left IX: 35% **Vermis IX: 11%**	-5.3; -53.3; -35.3	30	414.72
L Superior Frontal Gyrus: 14% **L Middle Frontal Gyrus: 22%** **L Precentral Gyrus: 9%**	-26.9; -0.5; 58.3	29	400.896
Cingulate Gyrus, anterior division: 43% **Cingulate Gyrus, posterior division: 16%**	-0.5; -10.1; 31.9	28	387.072
L Precentral Gyrus: 13% **L Postcentral Gyrus: 19%**	-62.9; -5.3; 36.7	27	373.248
L Postcentral Gyrus: 21%	-67.7; -7.7; 15.1	26	359.424
L Inferior Frontal Gyrus, pars triangularis: 7% **L Inferior Frontal Gyrus, pars opercularis: 15%**	-60.5; 16.3; 22.3	25	345.6
R Parahippocampal Gyrus, anterior division: 8% **RParahippocampal Gyrus, posterior division: 35%** **R Temporal Fusiform Cortex, posterior division: 23%**	23.5; -34.1; -23.3	24	331.776
Left Lateral Ventricle: 33% **Left Caudate: 54%**	-14.9; 23.5; 0.7	23	317.952

No activated clusters for H3a: CPHIV>Controls

H3a: CPHIV<Controls	Max X;Y;Z (MNI,mm)	Number of Voxels	Voxels mm3
Left Crus II: 83%	-24.5; -79.7; -47.3	31	428.544

H3b: Whole Group	Max X;Y;Z (MNI,mm)	Number of Voxels	Voxels mm3
Right Cerebral White Matter: 21% **Right Caudate: 45%** **Right Putamen: 16%** **Right Accumbens: 12%**	9.1; 9.1; -4.1	59	815.616
Left Cerebral White Matter: 24% **Left Cerebral Cortex: 11%** **Left Lateral Ventricle: 34%** **Left Caudate: 17%** **Left Accumbens: 11%**	-10.1; 6.7; -4.1	27	373.248

No activated clusters for H3b: CPHIV

H3b: Controls	Max X;Y;Z (MNI,mm)	Number of Voxels	Voxels mm3
Right Cerebral White Matter: 22% **Right Lateral Ventricle: 15%** **Right Caudate: 40%**	18.7; 11.5; -4.1	54	746.496
L Middle Frontal Gyrus: 18% **L Inferior Frontal Gyrus, pars opercularis: 11%** **L Precentral Gyrus: 25%**	-50.9; 9.1; 31.9	38	525.312
L Lateral Occipital Cortex, superior division: 59%	-29.3; -70.1; 43.9	32	442.368
L Frontal Pole: 21% **L Middle Frontal Gyrus: 9%** **L Inferior Frontal Gyrus, pars triangularis: 10%**	-53.3; 47.5; 10.3	24	331.776

No activated clusters for H3b: CPHIV>Controls

H3b: CPHIV<Controls	Max X;Y;Z (MNI,mm)	Number of Voxels	Voxels mm3
L Middle Frontal Gyrus: 15% **L Inferior Frontal Gyrus, pars opercularis: 13%** **L Precentral Gyrus: 29%**	-50.9; 9.1; 31.9	23	317.952

H4a: Whole Group	Max X;Y;Z (MNI,mm)	Number of Voxels	Voxels mm3
Left Cerebral White Matter: 13% **Left Cerebral Cortex: 15%** **Left Lateral Ventricle: 12%** **Right Cerebral White Matter: 12%** **Right Cerebral Cortex: 16%** **Right Lateral Ventricle: 11%**	-24.5; -46.1; 15.1	3527	48757.248
Occipital Fusiform Gyrus: 18% **Occipital Pole: 24%**	-17.3; -89.3; -11.3	768	10616.832
Cingulate Gyrus, posterior division: 25% **Precuneus Cortex: 33%**	1.9; -38.9; 48.7	444	6137.856
L Lateral Occipital Cortex, superior division: 59%	-29.3; -82.1; 36.7	210	2903.04
R Lateral Occipital Cortex, superior division: 56%	40.3; -77.3; 34.3	190	2626.56
L Precentral Gyrus: 16% **L Postcentral Gyrus: 24%**	-22.1; -36.5; 75.1	177	2446.848
R Postcentral Gyrus: 31%	21.1; -36.5; 72.7	107	1479.168
R Precentral Gyrus: 33% **R Postcentral Gyrus: 7%**	18.7; -14.9; 75.1	59	815.616
Left IX: 50%	-10.1; -48.5; -44.9	49	677.376
L Insular Cortex: 6% **L Temporal Pole: 30%**	-43.7; 13.9; -11.3	49	677.376
R Insular Cortex: 33% **R Temporal Pole: 16%**	45.1; 11.5; -8.9	48	663.552
R Temporal Pole: 27% **R Superior Temporal Gyrus, anterior division: 12%** **R Middle Temporal Gyrus, anterior division: 20%**	66.7; -0.5; -13.7	45	622.08
R Inferior Temporal Gyrus, temporooccipital part: 27% **R Temporal Occipital Fusiform Cortex: 41%**	45.1; -48.5; -18.5	38	525.312
Intracalcarine Cortex: 14% **Supracalcarine Cortex: 29%** **Occipital Pole: 14%**	6.7; -84.5; 10.3	37	511.488
R Middle Frontal Gyrus: 12% **R Precentral Gyrus: 9%**	57.1; 16.3; 34.3	29	400.896
L Intracalcarine Cortex: 18%	-19.7; -74.9; 5.5	29	400.896
L Lateral Occipital Cortex, superior division: 38%	-29.3; -62.9; 60.7	28	387.072
L Lingual Gyrus: 13% **L Temporal Fusiform Cortex, posterior division: 12%** **L Temporal Occipital Fusiform Cortex: 40%**	-24.5; -55.7; -13.7	28	387.072
L Precentral Gyrus: 24% **L Postcentral Gyrus: 43%**	-48.5; -14.9; 48.7	26	359.424

R Lateral Occipital Cortex, superior division: 57%	28.3; -62.9; 55.9	24	331.776
Frontal Pole: 51%	-19.7; 61.9; 29.5	23	317.952
R Lateral Occipital Cortex, inferior division: 63%	49.9; -72.5; 7.9	22	304.128

H4a: CPHIV	Max X;Y;Z (MNI,mm)	Number of Voxels	Voxels mm3
Left Lateral Ventricle: 30% **Right Lateral Ventricle: 26%** **Right Caudate: 15%**	16.3; 23.5; 5.5	313	4326.912
Left Cerebral White Matter: 33% **Left Lateral Ventricle: 62%**	-14.9; -31.7; 15.1	191	2640.384
Right Cerebral White Matter: 27% **Right Lateral Ventricle: 65%**	16.3; -19.7; 24.7	141	1949.184
L Occipital Fusiform Gyrus: 12% **L Occipital Pole: 38%**	-14.9; -89.3; -13.7	106	1465.344
R Precuneus Cortex: 41%	21.1; -58.1; 27.1	52	718.848
L Postcentral Gyrus: 41% **L Superior Parietal Lobule: 9%**	-22.1; -36.5; 75.1	41	566.784
Postcentral Gyrus: 14% **Cingulate Gyrus, posterior division: 11%** **Precuneus Cortex: 25%**	-0.5; -38.9; 63.1	36	497.664
R Postcentral Gyrus: 32% **R Superior Parietal Lobule: 6%**	21.1; -43.7; 75.1	31	428.544
R Occipital Fusiform Gyrus: 15% **R Occipital Pole: 19%**	23.5; -89.3; -11.3	30	414.72
Right Cerebral White Matter: 11% **Right Cerebral Cortex: 21%**	1.9; -38.9; 3.1	25	345.6
Right Cerebral White Matter: 31% **Right Lateral Ventricle: 19%** **Right Hippocampus: 43%**	25.9; -38.9; 3.1	21	290.304
L Precentral Gyrus: 10% **L Postcentral Gyrus: 9%**	-22.1; -26.9; 77.5	21	290.304

H4a: Controls	Max X;Y;Z (MNI,mm)	Number of Voxels	Voxels mm3
Left Cerebral White Matter: 14% **Left Cerebral Cortex: 14%** **Left Lateral Ventricle: 13%** **Right Lateral Ventricle: 13%**	-26.9; -43.7; 12.7	1659	22934.02

R Lateral Occipital Cortex, superior division: 28% **R Precuneus Cortex: 25%** **R Cuneal Cortex: 10%**	16.3; -77.3; 39.1	539	7451.136
Cingulate Gyrus, posterior division: 39% **Precuneus Cortex: 33%**	1.9; -34.1; 29.5	265	3663.36
L Lateral Occipital Cortex, inferior division: 10% **L Occipital Fusiform Gyrus: 34%** **L Occipital Pole: 8%**	-19.7; -89.3; -11.3	101	1396.224
L Occipital Pole: 54%	-5.3; -94.1; -1.7	82	1133.568
L Temporal Pole: 25% **L Frontal Orbital Cortex: 12%**	-43.7; 16.3; -13.7	51	705.024
L Angular Gyrus: 43% **L Lateral Occipital Cortex, superior division: 91%**	-60.5; -60.5; 19.9	46	635.904
R Lingual Gyrus: 11% **R Occipital Pole: 37%**	13.9; -91.7; -1.7	42	580.608
R Lateral Occipital Cortex, inferior division: 10% **R Occipital Fusiform Gyrus: 50%**	33.1; -74.9; -13.7	41	566.784
R Parahippocampal Gyrus, posterior division: 23% **R Lingual Gyrus: 22%**	23.5; -36.5; -20.9	40	552.96
Vermis VI: 28% **Right VI: 42%**	1.9; -74.9; -23.3	40	552.96
R Lateral Occipital Cortex, superior division: 68%	47.5; -67.7; 39.1	39	539.136
R Lingual Gyrus: 21% **R Occipital Fusiform Gyrus: 30%**	18.7; -82.1; -16.1	39	539.136
R Inferior Temporal Gyrus, temporooccipital part: 39% **R Temporal Occipital Fusiform Cortex: 35%**	49.9; -48.5; -18.5	35	483.84
Frontal Pole: 30% **Superior Frontal Gyrus: 19%**	1.9; 54.7; 27.1	28	387.072
Paracingulate Gyrus: 52% **Cingulate Gyrus, anterior division: 22%**	-0.5; 16.3; 39.1	26	359.424
R Postcentral Gyrus: 38%	21.1; -36.5; 72.7	23	317.952
L Lateral Occipital Cortex, superior division: 10% **L Lateral Occipital Cortex, inferior division: 14%** **L Occipital Pole: 35%**	-36.5; -94.1; 10.3	22	304.128

No activated clusters for H4a: CPHIV>Controls

No activated clusters for H4a: CPHIV<Controls

No activated clusters for H4b

H4c: Whole Group	Max X;Y;Z (MNI,mm)	Number of Voxels	Voxels mm3
Occipital Pole: 10%	16.3; -94.1; 5.5	8079	111684.096
Left Cerebral White Matter: 13% **Left Putamen: 11%** **Right Cerebral White Matter: 15%** **Right Cerebral Cortex: 13%** **Right Caudate: 7%** **Right Putamen: 11%**	21.1; 4.3; -8.9	2718	37573.632
R Frontal Pole: 11% **R Middle Frontal Gyrus: 15%** **R Precentral Gyrus: 15%**	42.7; 9.1; 27.1	1464	20238.336
Paracingulate Gyrus: 34% **Cingulate Gyrus, anterior division: 27%**	-2.9; 37.9; 7.9	1004	13879.296
L Frontal Pole: 10% **L Middle Frontal Gyrus: 16%** **L Precentral Gyrus: 15%**	-48.5; 35.5; 24.7	811	11211.264
Cingulate Gyrus, anterior division: 10% **Cingulate Gyrus, posterior division: 45%**	-2.9; -31.7; 29.5	518	7160.832
L Frontal Pole: 33% **L Frontal Orbital Cortex: 36%**	-24.5; 33.1; -13.7	139	1921.536
L Insular Cortex: 28% **L Frontal Orbital Cortex: 10%**	-29.3; 28.3; 3.1	101	1396.224
L Middle Frontal Gyrus: 18% **L Precentral Gyrus: 29%**	-31.7; -5.3; 53.5	94	1299.456
Right Crus II: 26% **Right VIIb: 46%** **Right VIIIa: 9%**	30.7; -74.9; -52.1	78	1078.272
R Superior Frontal Gyrus: 26% **R Middle Frontal Gyrus: 23%**	25.9; 18.7; 58.3	50	691.2
R Lateral Occipital Cortex, superior division: 12% **R Lateral Occipital Cortex, inferior division: 41%**	45.1; -72.5; 7.9	41	566.784
R Frontal Pole: 62%	40.3; 59.5; 7.9	28	387.072
R Parahippocampal Gyrus, posterior division: 32% **R Temporal Fusiform Cortex, posterior division: 26%** **R Temporal Occipital Fusiform Cortex: 14%**	23.5; -36.5; -18.5	25	345.6
R Frontal Pole: 51%	28.3; 57.1; -8.9	24	331.776
R Precuneus Cortex: 25%	21.1; -50.9; 22.3	23	317.952
L Superior Frontal Gyrus: 16% **L Middle Frontal Gyrus: 20%**	-31.7; 4.3; 67.9	23	317.952

H4c: CPHIV	Max X;Y;Z (MNI,mm)	Number of Voxels	Voxels mm3
L Lateral Occipital Cortex, superior division: 17% **L Occipital Pole: 28%**	-19.7; -98.9; 24.7	1141	15773.18
Left Cerebral White Matter: 13% **Left Putamen: 24%** **Right Cerebral White Matter: 11%** **Right Putamen: 20%**	-22.1; 6.7; -6.5	742	10257.41
R Middle Frontal Gyrus: 15% **R Inferior Frontal Gyrus, pars opercularis: 17%** **R Precentral Gyrus: 21%**	47.5; 9.1; 22.3	354	4893.696
Left Crus I: 50% **Left Crus II: 26%**	-38.9; -62.9; -42.5	319	4409.856
R Lateral Occipital Cortex, superior division: 50%	28.3; -65.3; 43.9	261	3608.064
L Occipital Fusiform Gyrus: 36%	-36.5; -79.7; -13.7	251	3469.824
R Occipital Pole: 55%	16.3; -94.1; 5.5	207	2861.568
R Middle Temporal Gyrus, temporooccipital part: 27% **R Inferior Temporal Gyrus, temporooccipital part: 29%**	59.5; -50.9; -8.9	160	2211.84
Cingulate Gyrus, posterior division: 68%	-2.9; -31.7; 29.5	141	1949.184
Paracingulate Gyrus: 27% **Cingulate Gyrus, anterior division: 49%**	1.9; 37.9; 7.9	114	1575.936
Right Crus I: 22% **Right Crus II: 66%**	42.7; -60.5; -44.9	57	787.968
R Frontal Pole: 37% **R Frontal Orbital Cortex: 41%**	23.5; 28.3; -16.1	53	732.672
R Frontal Pole: 50% **R Middle Frontal Gyrus: 8%** **R Inferior Frontal Gyrus, pars triangularis: 9%**	52.3; 40.3; 17.5	53	732.672
R Superior Parietal Lobule: 22% **R Supramarginal Gyrus, posterior division: 28%**	40.3; -41.3; 46.3	50	691.2
L Middle Temporal Gyrus, temporooccipital part: 11% **L Inferior Temporal Gyrus, temporooccipital part: 38%** **L Lateral Occipital Cortex, inferior division: 22%**	-55.7; -60.5; -11.3	38	525.312
L Temporal Fusiform Cortex, posterior division: 32% **L Temporal Occipital Fusiform Cortex: 37%**	-34.1; -48.5; -18.5	38	525.312
R Insular Cortex: 20% **R Frontal Orbital Cortex: 24%**	35.5; 33.1; -1.7	24	331.776

H4c: Controls	Max X;Y;Z (MNI,mm)	Number of Voxels	Voxels mm3
R Insular Cortex: 4% **R Frontal Orbital Cortex: 5%** **R Frontal Operculum Cortex: 2%**	37.9; 25.9; -1.7	1973	27274.75
Superior Frontal Gyrus: 6% **Paracingulate Gyrus: 33%** **Cingulate Gyrus, anterior division: 24%**	-7.7; 18.7; 46.3	969	13395.46
L Middle Frontal Gyrus: 17% **L Inferior Frontal Gyrus, pars opercularis: 7%** **L Precentral Gyrus: 19%**	-48.5; 4.3; 22.3	799	11045.38
L Occipital Fusiform Gyrus: 6% **L Occipital Pole: 31%**	-7.7; -96.5; -4.1	637	8805.888
L Superior Frontal Gyrus: 23% **L Middle Frontal Gyrus: 20%**	-26.9; 16.3; 65.5	357	4935.168
R Superior Frontal Gyrus: 11% **R Middle Frontal Gyrus: 19%** **R Precentral Gyrus: 21%**	28.3; 16.3; 60.7	335	4631.04
R Middle Frontal Gyrus: 11% **R Inferior Frontal Gyrus, pars opercularis: 20%** **R Precentral Gyrus: 22%**	42.7; 9.1; 27.1	299	4133.376
R Lingual Gyrus: 14% **R Occipital Fusiform Gyrus: 17%** **R Occipital Pole: 20%**	16.3; -91.7; 5.5	273	3773.952
R Lateral Occipital Cortex, superior division: 51%	33.1; -67.7; 24.7	247	3414.528
R Superior Parietal Lobule: 27% **R Supramarginal Gyrus, anterior division: 7%** **R Supramarginal Gyrus, posterior division: 8%** **R Angular Gyrus: 7%**	52.3; -34.1; 55.9	186	2571.264
L Lateral Occipital Cortex, superior division: 55%	-29.3; -70.1; 43.9	160	2211.84
L Lateral Occipital Cortex, inferior division: 16% **L Occipital Fusiform Gyrus: 11%**	-34.1; -79.7; -13.7	152	2101.248
L Supramarginal Gyrus, anterior division: 15% **L Supramarginal Gyrus, posterior division: 27%**	-48.5; -46.1; 55.9	149	2059.776
R Inferior Temporal Gyrus, temporooccipital part: 39% **R Lateral Occipital Cortex, inferior division: 12%**	52.3; -55.7; -11.3	96	1327.104
Cingulate Gyrus, posterior division: 60% **Precuneus Cortex: 11%**	1.9; -31.7; 29.5	94	1299.456
L Inferior Temporal Gyrus, temporooccipital part: 39% **L Lateral Occipital Cortex, inferior division: 14%** **L Temporal Occipital Fusiform Cortex: 8%**	-50.9; -60.5; -13.7	90	1244.16

L Frontal Pole: 31% **L Frontal Orbital Cortex: 36%**	-38.9; 35.5; -11.3	88	1216.512
R Frontal Pole: 36% **R Middle Frontal Gyrus: 12%** **R Inferior Frontal Gyrus, pars triangularis: 13%**	40.3; 37.9; 7.9	79	1092.096
Cingulate Gyrus, anterior division: 42% **Cingulate Gyrus, posterior division: 8%**	1.9; -2.9; 29.5	65	898.56
Right Crus I: 54% **Right Crus II: 22%**	42.7; -62.9; -37.7	64	884.736
L Lateral Occipital Cortex, superior division: 53%	-19.7; -65.3; 60.7	51	705.024
Left Crus I: 18% **Left Crus II: 63%** **Left VIIb: 14%**	-36.5; -72.5; -52.1	46	635.904
Cingulate Gyrus, anterior division: 40%	-5.3; 4.3; 27.1	27	373.248
Cingulate Gyrus, posterior division: 20% **Precuneus Cortex: 46%**	-2.9; -53.3; 15.1	27	373.248
Right Cerebral White Matter: 26% **Right Cerebral Cortex: 11%** **Right Thalamus: 24%**	9.1; -26.9; 0.7	24	331.776
Left IX: 15% **Vermis IX: 31%** **Vermis X: 13%**	1.9; -53.3; -35.3	24	331.776
Right VI: 28% **Right Crus I: 72%**	33.1; -67.7; -28.1	23	317.952

No activated clusters for H4c: CPHIV>Controls

H4c: CPHIV<Controls	Max X;Y;Z (MNI,mm)	Number of Voxels	Voxels mm3
L Superior Frontal Gyrus: 20% **L Middle Frontal Gyrus: 21%**	-24.5; 28.3; 39.1	45	622.08
L Superior Frontal Gyrus: 20% **L Paracingulate Gyrus: 13%**	-7.7; 23.5; 51.1	33	456.192
L Superior Frontal Gyrus: 22% **L Middle Frontal Gyrus: 34%**	-29.3; 28.3; 48.7	33	456.192